Kaunas University of Technology

Faculty of Mathematics and Natural Sciences

Evaluation and Analysis of Secondary Cancer Risks Based on Irradiation Doses to Organs at Risk for Head and Neck Cancer Cases

Master's Final Degree Project

Sundus Osman Mohammed Osman

Project author

Assoc. Prof. Dr. Jurgita Laurikaitienė

Supervisor

Kaunas, 2025

Kaunas University of Technology

Faculty of Mathematics and Natural Sciences

Evaluation and Analysis of Secondary Cancer Risks Based on Irradiation Doses to Organs at Risk for Head and Neck Cancer Cases

Master's Final Degree Project

Medical Physics (6213GX001)

Sundus Osman Mohammed Osman

Project author

Assoc. Prof. Dr. Jurgita Laurikaitienė

Supervisor

Assoc. Prof. Dr. Vytautas Stankus

Reviewer

Kaunas University of Technology

Faculty of Mathematics and Natural Science

Sundus Osman Mohammed Osman

Evaluation and Analysis of Secondary Cancer Risks Based on Irradiation Doses to Organs at Risk for Head and Neck Cancer Cases

Declaration of Academic Integrity

I hereby declare that this Master's Final Degree Project, titled "Evaluation and Analysis of Secondary Cancer Risks Based on Irradiation Doses to Organs at Risk for Head and Neck Cancer Cases", has been written independently and reflects my own work.

I confirm that

1. All data, analyses, and interpretations presented in this thesis are my own, except where explicitly stated otherwise and appropriately cited.

2. I have fully acknowledged all sources and references used in accordance with academic integrity and copyright laws.

3. No part of this work has been plagiarized or submitted previously for academic credit at any institution.

4. I have not paid anyone to prepare or writing any part of this thesis.

5. I understand that any breach of academic integrity may result in academic sanctions according to the regulations of Kaunas University of Technology.

Sundus Osman Mohammed Osman

Confirmed electronically

Sundus Osman Mohammed Osman. Evaluation and Analysis of Secondary Cancer Risks Based on Irradiation Doses to Organs at Risk for Head and Neck Cancer Cases /Supervisor Assoc. Prof. Dr. Jurgita Laurikaitienė; Faculty of Mathematics and Natural Science, Kaunas University of Technology.

Study field and area (study field group): Medical Technologies (Health Sciences)

Keywords: head and neck cancer, excess absolute risk (EAR), anthropomorphic phantom, out-of-field irradiation doses

Kaunas, 2025, 68 p.

Summary

Head and neck cancer (HNC) presents complex treatment challenges due to the proximity of tumours to critical organs, increasing the risk of radiation-induced complications. This study showed how demographic, anatomical, and clinical factors are influenced by radiation dose delivery and the associated risk of secondary cancers. The analysis indicated that HNC incidence was highest among men aged 60–69, with the oral cavity and oropharynx being the most affected sites. Statistical analysis showed that depending on the patient's age, the irradiation doses of organs such as the oesophagus and parotid glands differ, while gender had the least impact on the change in irradiation dose of critical organs. The assessment of Excess Absolute Risk (*EAR*) revealed a consistent trend that patients with more advanced disease stages particularly those classified as Stage IV (T4_N1_M0) faced significantly higher long-term risks.

To assess the accuracy of treatment planning system (TPS) dose estimations, out-of-field doses were measured using a cylindrical ionization chamber (PTW 30013) positioned within the SHANE anthropomorphic phantom. These measured values were compared with TPS-calculated doses using two algorithms: the Anisotropic Analytical Algorithm (AAA) and *Acuros* XB. Both algorithms exhibited consistent underestimation of out-of-field doses, with the most significant discrepancy 57.1 % observed in Channel 4 (spinal cord region) at 0 cm using the *Acuros* XB algorithm. Moreover, at distances beyond 10 cm from the treatment field edge, underestimations remained notable, particularly in Channels 3 and 4. These findings highlight the limitations of TPS algorithms in accurately predicting peripheral dose, reinforcing the importance of incorporating phantom-based dose measurements into routine radiotherapy planning to ensure reliable dose assessment for organs at risk (OARs), ultimately contributing to improved long-term patient outcomes.

Sundus Osman Mohammed Osman. Antrinio vėžio rizikos sąsajos su kritinių organų apšvita vertinimas ir analizė nagrinėjant galvos ir kaklo vėžio atvejus. Magistro baigiamasis projektas / vadovas doc. dr. Jurgita Laurikaitienė; Kauno technologijos universitetas, Matematikos ir gamtos mokslų fakultetas.

Studijų kryptis ir sritis (studijų krypčių grupė): Medicinos technologijos (Sveikatos mokslai).

Reikšminiai žodžiai: galvos ir kaklo vėžys, antrinė vėžio rizika, antropomorfinis fantomas, apšvitos dozės už gydymo lauko ribos

Kaunas, 2025. 68 p.

Santrauka

Galvos ir kaklo vėžio gydymas ir jo planavimas yra sudėtingas procesas, dėl šalia naviko esančių kritinių organų, kurių apšvita atitinkamai gali padidinti jonizuojančiosios spinduliuotės sukeltų komplikacijų riziką. Šis tyrimas parodė, kaip galvos ir kaklo vėžiu sergančio paciento demografiniai, anatominiai ir klinikiniai veiksniai yra susiję su apšvita jonizuojančiąja spinduliuota ir jos sukelta antrine vėžio rizika. Pastebėta, kad sergamumas galvos ir kaklo vėžio buvo didžiausias tarp 60–69 metų vyrų, o dažniausiai pažeidžiamos burnos ertmės ir burnaryklės sritys. Statistinė analizė parodė, kad priklausomai nuo paciento amžiaus, gali keistis tokių organų kaip stemplė ir paausinės liaukos apšvita, kai tuo tarpu lytis kritinių organų apšvitos kitimui žymios įtakos neturėjo. Be to, antrinės vėžio rizikos vertinimas parodė, kad IV stadijos pacientams (T4_N1_M0) ilgalaikė rizika buvo žymiai didesnė, lyginant ją su kitų stadijų pacientais.

Siekiant įvertinti gydymo planavimo sistemos (TPS) dozių skaičiavimo tikslumą, už laukelio ribų gautos dozės buvo išmatuotos naudojant cilindrinę jonizacinę kamerą (PTW 30013), įstatytą į antropomorfinį fantomą SHANE. Šios išmatuotos vertės buvo palygintos su TPS apskaičiuotomis dozėmis, naudojant du skirtingus algoritmus: anisotropinį analitinį algoritmą (AAA) ir Acuros XB. Abu algoritmai parodė tendenciją nuvertinti dozes už apšvitinimo laukelio ribų, o didžiausias neatitikimas – 57,1 % – buvo užfiksuotas 4 kanale (nugaros smegenų srityje), esant 0 cm atstumui, naudojant Acuros XB algoritmą. Be to, esant didesniam nei 10 cm atstumui nuo apšvitinimo lauko krašto, nuvertinimai išliko reikšmingi, ypač 3 ir 4 kanaluose. Šie rezultatai parodo TPS algoritmų ribotumus tiksliai prognozuojant periferines dozes, todėl rekomenduojama integruoti fantomu pagrįtus dozių matavimus į kasdienę radioterapijos planavimo praktiką, siekiant užtikrinti patikimą rizikingų organų (OAR) dozių įvertinimą ir pagerinti ilgalaikius pacientų gydymo rezultatus.

Table of contents

List of figures

List of tables

List of abbreviations and terms

Abbreviations:

HNC – Head and neck cancer;

HNSCC – Head and neck squamous cell carcinoma;

IMRT – Intensity-modulated radiation therapy;

VMAT – Volumetric modulated arc therapy;

OARs – Organs at risk;

CBCT – Cone-beam computed tomography;

SPC – second primary cancer;

Gy – Gray (unit of radiation dose);

HPV – Human papilloma virus;

p – *p*-value (in statistical tests);

EAR – Excess absolute risk;

TNM – Tumour-Node-Metastasis (classification system);

DNA – Deoxyribonucleic acid;

AAA – Anisotropic analytical algorithm;

AC – *Acuros* XB algorithm.

Terms:

Out-of-Field Doses – Unintended radiation exposure to tissues and organs outside the primary treatment area during radiation therapy.

Phantom – A model used in radiation therapy to simulate human tissue and evaluate dose distributions accurately.

Anthropomorphic phantoms – Used in medical imaging and radiation treatment to imitate tissue interactions with radiation for enhanced dosimetry and treatment planning, anthropomorphic phantoms are models that mimic human body form and features.

Excess absolute risk (EAR) – The increase in the absolute risk of a secondary effect, expressed as the additional number of cases per unit of population.

Introduction

Head and neck cancer (HNC) represents a significant public health challenge, accounting for approximately 550,000 new cases and 300,000 deaths annually worldwide these malignancies originate from various anatomical sites, including the oral cavity, pharynx, larynx, and salivary glands, and are associated with substantial morbidity and mortality. The challenges of treating HNC come from the complicated structure of the head and neck area, where the tumour's position is often near important organs and parts that are crucial for essential body functions [1]. External beam radiation therapy is a cornerstone of HNC management, effectively employed in both curative and palliative contexts. However, the precision of dose calculation and delivery issues remain a problem and critical concern [2]. It is known that treatment planning systems (TPS) may exhibit discrepancies (from 30 % to 60 %) in the accurate calculation of radiation doses to organs at risk (OAR) or so-called out-of-field doses, which may be harmful through overexposure to healthy tissues [3]. In particular, exposure to out-of-field doses affecting organs and tissues outside the treatment area has become increasingly concerning, as it may result in unintended long-term effects [4]. Due to this reason, evaluation of secondary cancer risks based on patient-specific factors induced by irradiation of healthy tissues is an essential and important step in external beam radiotherapy for the treatment plan optimization adapting dose limitation constraints [5]. Therefore, addressing mentioned challenges requires careful consideration of the patient-specific factors to ensure the overall safety and effectiveness of radiation therapy.

The aim of this study is to evaluate and analyse the impact of patient-specific factors on secondary cancer risk for head and neck cancer cases based on comparison of 3D treatment planning system *Eclipse* calculated irradiation doses to organs at risk and dosimetry measurements, preparing strategies for the clinically used dose limitations.

The tasks:

- To analyse the main dosimetry data for the cohort of head and neck cancer patients, including an evaluation of patient-specific factors, like gender, age and stage-based differences related to radiation doses to organs at risk (OARs).
- To estimate the risk of secondary cancer and calculate the excess absolute risk (*EAR*) based on 3D treatment planning system (TPS) *Eclipse* dosimetry data.
- To measure and analyse anthropomorphic phantom *SHANE* based out-of-field doses of 1D cylindrical ionisation chamber, comparing with the doses calculated by TPS, employing different algorithms.
- To recommend potential modifications to clinically used dose limitation constraints based on out-of-field doses measurements and secondary cancer risk evaluation.

1.Literature review

1.1. Head and neck cancer

Head and neck cancers (HNCs) represent a significant global health challenge, ranking as the sixth most prevalent cancer type worldwide, with approximately 550,000 new cases diagnosed annually and an estimated 300,000 deaths [6]. Most head and neck cancers are a type called squamous cell carcinoma (HNSCC) [7], arising from various anatomical sites (Fig. 1), including the pharynx, larynx, paranasal sinuses, nasal cavity, oral cavity, and salivary glands [3], the ethology and epidemiology of these cancers are becoming increasingly complex. Traditionally, tobacco use, and chronic alcohol consumption have been recognized as the main risk factors for HNSCC [4], while the increasing incidence of oropharyngeal cancers, particularly among younger individuals, has highlighted the increasing importance of human papillomavirus (HPV) infection. Moreover, studies have shown that HPV, especially type 16, is associated with a significant proportion (60-70 %) of newly diagnosed oropharyngeal cancers in the United States and certain regions of the European Union [8]. Although HPV-16 is the most well-established causal agent, other types of HPV, including 18, 31, and 33, also contribute to the development of these malignancies [7].

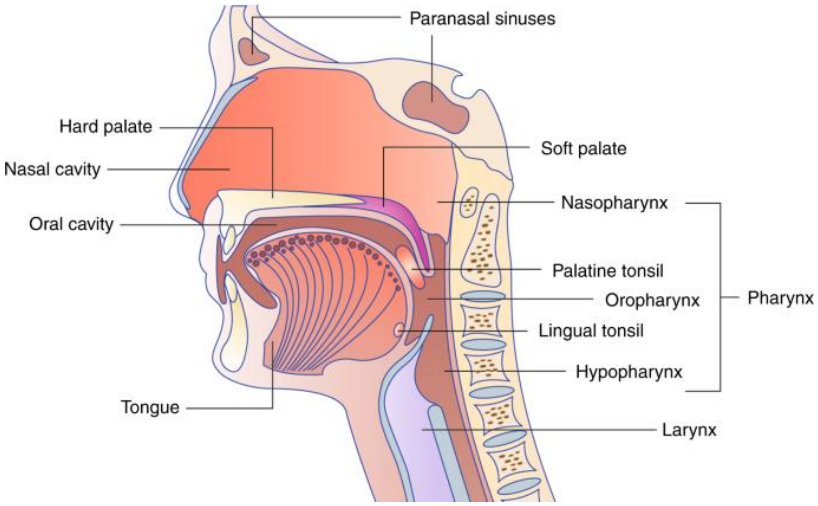

Fig. 1. Anatomical view of the head and neck [9]

Given the heterogeneity of HNC and the varying impact of risk factors, accurate staging is crucial to guide treatment decisions and predict survival prognosis. The TNM staging system, managed by the American Joint Committee on Cancer (AJCC), offers a standardized structure for categorizing the anatomical scope of the disease. This system assesses the size and local reach of the primary tumour (T), the presence and extent of regional lymph node spread (N), and the existence of distant metastases (M) [10]. Subsequently, TNM classifications are amalgamated to determine an overall stage, ranging from stage I (early stage, localized disease) to stage IV (advanced disease with widespread dissemination) [11]. Many research studies have shown a significant relationship between the TNM stage and survival rates for head and neck cancer (HNC), where higher stages generally correspond to poorer outcomes. Consequently, the stage plays a crucial role in deciding the most suitable treatment strategy, varying from single-modality interventions (e.g., surgery or radiation) for early-stage tumours to aggressive multimodal treatments (e.g., chemoradiation followed by surgery) for advanced disease [12].

1.2. Radiation therapy

In head and neck cancer (HNC), complex anatomy and close proximity of organs at risk (OARs) make radiation therapy (RT) a critical component that is frequently used in combination with surgery, chemotherapy, and novel systemic agents as a multidisciplinary strategy [13]. RT contributes to about 40% of cancer cures, which destroy cancer cells using high energy particles or X-ray photons irradiating the cells to damage deoxyribonucleic acid (DNA) damage and consequently, death. However, in spite of these advances in RT, local recurrence, which occurs in about half of HNC patients within 3 years of treatment, remains one of the greatest limitations [14]. Furthermore, RT is associated with a variety of both acute and late toxicity, further stressing the need for additional optimization of treatment approaches. RT can be delivered by various methods including brachytherapy (intracavity irradiation) and external beam radiation therapy (EBRT); EBRT is the most common method used, with a cumulative dose usually of 60 – 70 cGy for 180–200 cGy/day daily fractions [2].

1.3. External beam radiation therapy techniques

External beam radiation therapy (EBRT) is a fundamental modality in the treatment of neoplasms of all types, which utilizes ionizing radiation to disassemble the cellular structure of malignant tissues. The main aim of EBRT is to irradiate the tumour with a known vibration dose and to preserve the surrounding healthy tissue and hence to limit the possible occurrence of side effects. The biology of radiation is primarily mediated by DNA damage, which initiates cellular processes culminating in either apoptosis, senescence, or mitotic catastrophe [15]. Recent advances in EBRT focus on precision, tailored treatment and effectiveness [16]. For instance, stereotactic body radiation therapy (SBRT) is a state-of-the-art radiation oncology technique that concentrates on the delivery of extremely high radiation doses directly to tumours and has gained a lot of attention lately. Advanced imaging, such as cone-beam computed tomography or planning CT simulation, enables SBRT with appreciable accuracy in tumour localization, and it is especially active in cases of small distinct tumours in the complex body locations [17]. Treatment usually consists of heterogeneous doses of ionizing radiation during a relatively few sessions, usually one to five fractions.

This model suggests that it may be possible to improve tumour control by applying large doses in a smaller number of sessions. On-clinical trials support the strong clinical benefits of SBRT in particular in the treatment of early-stage non-small cell lung cancer (NSCLC) (Fig. 2) [18]. For example, local control rates are reported to be over 90 %, which means that SBRT can be considered an alternative to surgery. In addition, SBRT has favourable toxicity, with reduced rates of complications such as respiratory complaint and pain, compared to standard fractionated (1.8 or 2.0 Gy/f) radiation therapies [19].

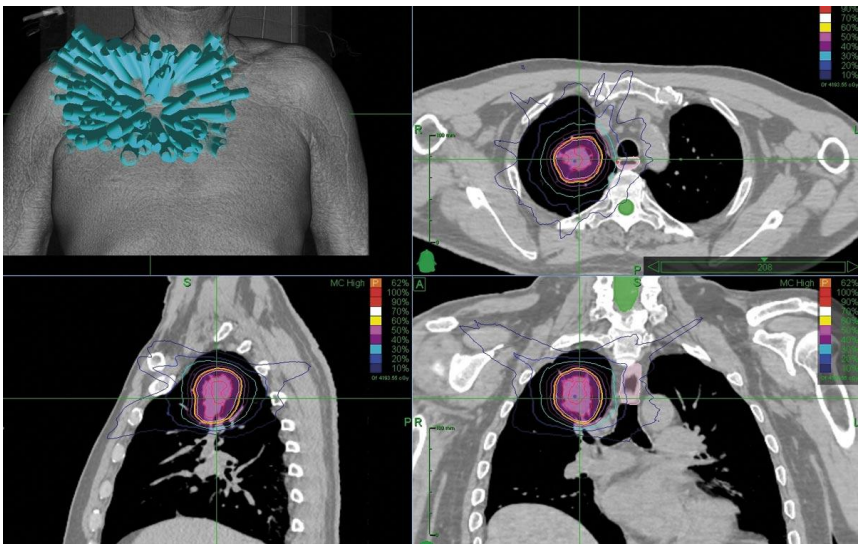

Fig. 2. Stereotactic body radiation therapy [18]

However, the appropriate implementation of SBRT requires a multidisciplinary team of radiation oncologists, medical physicists, and imaging experts to pay meticulous attention to every detail of SBRT delivery. In addition, the long-term effects, such as the risk of radiation-induced injury to the adjacent healthy tissues and the risk of second cancers, remain to be investigated to establish the safety and efficacy of the treatment [19].

The second more sophisticated personalized patient treatment method in addition to gating in which radiation plans are altered during therapy in response to real-time changes in the patient anatomy and response to the tumour, is referred to as adaptive radiation therapy (ART) [20]. Unlike conventional methods such as stereotactic body radiation therapy (SBRT) or stereotactic radiosurgery (SRS), which utilize a fixed treatment plan throughout the entire course. ART offers a higher degree of flexibility, assuring accuracy of the treatment, for example, due to the moving tumours [21]. The process begins (Fig. 3) with an initial planning session, where baseline imaging such as CT, magnetic resonance imaging (MRI), or positron emission tomography (PET) is used to delineate the target volumes and adjacent organs at risk.

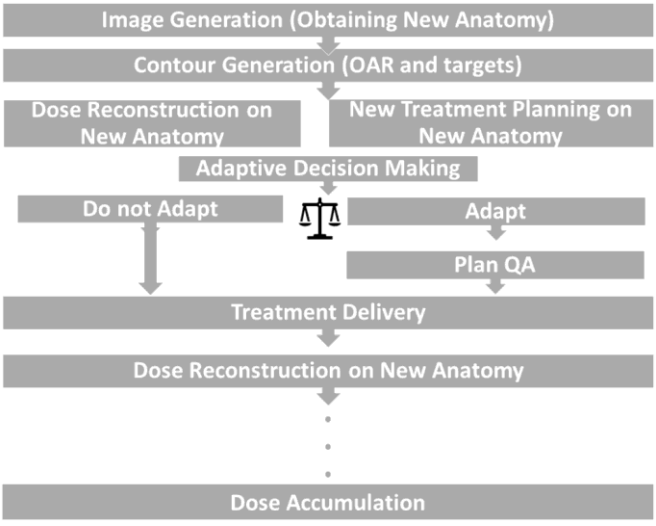

Fig. 3. Overview of the adaptive radiation therapy process [21]

Throughout treatment, continuous imaging modalities like cone-beam computed tomography (CBCT), Magnetic resonance imaging (MRI), or ultrasound are employed to monitor any changes in tumour size, shape, or position, as well as variations in the surrounding healthy tissues [22]. This

ongoing assessment allows clinicians to detect deviations from the original plan promptly. Based on the latest imaging data, an adaptive plan is generated either in real-time (online ART) or between treatment sessions (offline ART) to adjust dose distributions and ensure accurate delivery tailored to the patient's current anatomy. In online ART, modifications are made immediately during the treatment session, providing a highly personalized approach, especially beneficial in cases with significant tumour movement, such as lung tumours affected by respiratory motion or post-surgical breast cancer. This workflow involves re-optimizing the treatment plan based on the current imaging, verifying the modifications, and implementing the updated plan for subsequent treatment fractions. The entire process aims to maximize tumour control while minimizing exposure to healthy tissues, thereby improving treatment efficacy and reducing toxicity [21].
Even though SBRT and ART are complicated, they are built on 3D radiotherapy, which came from three-dimensional conformal radiation therapy (3D-CRT) in the 1990s and was a major step forward in radiotherapy, mainly because of the use of computed tomography (CT) imaging in planning treatments [23].

1.3.1. Three-dimensional conformal radiation therapy

Three-dimensional conformal radiation therapy (3D CRT) technology helps clearly define the areas to be treated and the nearby organs that could be affected, allowing for treatment plans that better match the shape of tumour with the radiation dose. The addition of multi-leaf collimators (MLCs) improved how well the radiation dose fits the tumour and protects nearby healthy tissues, leading to more focused treatment methods. The introduction of multi-leaf collimators (MLCs) further enhanced dose conformity and sparing of adjacent normal tissues, allowing for more targeted irradiation strategies [24]. Even with these advancements, 3D-CRT struggled to protect nearby organs at risk (OARs) effectively, particularly when dealing with complicated or oddly shaped target areas, which made planning the treatment difficult. Consequently, although 3D-CRT marked a significant step toward personalized radiotherapy, its constraints underscored the need for further technological evolution in treatment planning toward more sophisticated techniques such as intensity-modulated radiation therapy (IMRT) or volumetric- modulated arc therapy (VMAT) [25].

1.3.2. Intensity-modulated radiation therapy

In 1982, Brahme et al. [27] of the Karolinska institute in Stockholm published the basic concept for intensity modulated radiation therapy (IMRT). They developed the strategy of beam-intensity modulation in rotational therapy for uniform distribution to a toroidal target [26]. Unlike traditional forward dose planning technique where intensities of the beams are prescribed before computing doses, they treated the problem as an inverse one. That is, instead of designing the dose distribution based on a given beam pattern, the beam pattern itself is designed from a desired dose distribution, commonly called "inverse planning", wherein the desired dose distribution is introduced as an initial condition and the relevant beam intensity is calculated from the solution of an integral equation. IMRT has proven to be a game changer in radiation treatment, which is capable of modulating the intensity of the beam and thus giving rise to a steep dose gradient and highly conformal dose distribution that 3D-CRT cannot offer [27]. This innovative capacity allows clinicians to optimize coverage of irregular tumour shapes, enhancing the likelihood of tumour control and preserving critical organs at risk (OARs). By utilizing multiple beam angles, IMRT contours the radiation dose around the target, thus significantly improving tumour coverage while minimizing radiation exposure to surrounding healthy tissues, shown in (Fig. 4) [26].

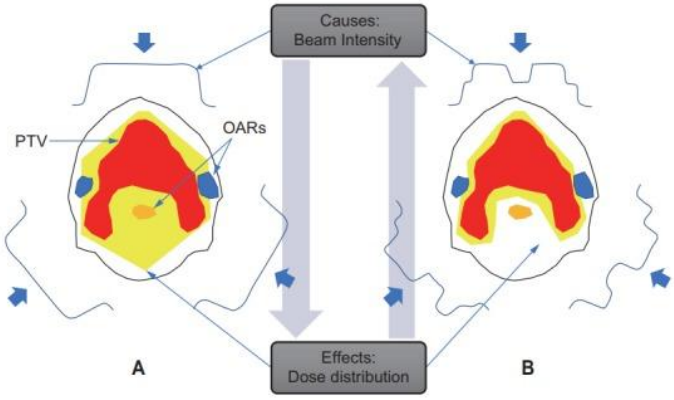

Fig. 4. 3D conformal radiation therapy (3D-CRT) (A) and intensity-modulated radiation therapy (IMRT) (B), featuring diagrams of forward planning versus inverse planning [26]

The potential heightened risk of radiation-induced secondary malignancies presents a concern regarding intensity-modulated radiation therapy (IMRT). IMRT typically necessitates 2 to 5 times more monitor units, thereby augmenting total body exposure to stray radiation. These factors are believed to elevate the likelihood of future cancer development. In comparison to conventional radiotherapy, IMRT may nearly double the likelihood of subsequent malignancies, thereby elevating the estimated risk for patients surviving a decade from approximately 1 % to nearly 1.75 % [24, 28]. A recent study [29] utilising Surveillance, Epidemiology, and End Results (SEER) data concerning head-and-neck cancer patients treated from 1992 to 2012 revealed that the annual incidence of secondary malignancies during the IMRT period (2010–2012) was consistently lower than that of patients who did not receive radiation therapy. This indicates that, relative to previous 3D-CRT methods (1992–2009), there is insufficient evidence to support an escalation in secondary malignancies associated with IMRT [30].

1.3.3. Volumetric Modulated Arc Therapy

Volumetric modulated arc therapy (VMAT) is an advanced rotational radiotherapy technique (VMAT). This technique is becoming more well-known since it can precisely target tumours while maintaining nearby healthy tissue and performs this much faster than more traditional treatments. Unlike conventional radiation treatment planning techniques using fixed beams targeted at a tumour [31]. VMAT makes use of a radiation device rotating around the patient in a continuous arc at the same time modulating intensity of the beam (Fig. 5). Several factors are changed in real time over this rotation: it updates configuration of the beam using multi-leaf collimators (MLCs), changes the dose rate, and controls the gantry's movement speed [32].

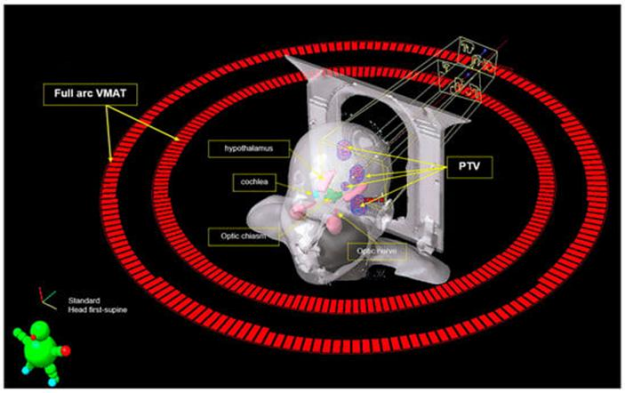

Fig. 5. Volumetric modulated arc therapy [33]

Even in cases with uneven outlines, this dynamic technique enables the exact modification of the radiation dosage, closely conformingly to the form of the tumour. Modern algorithms used in the design process enhance parameters to increase tumour coverage while protecting nearby organs [33].

Studies [31, 34] have shown how well the doses distribution is calculated using VMAT for different types of cancer. It was observed that greatly reducing the radiation dosage to vital tissues like salivary glands and the spinal cord, VMAT shows similar or better tumour coverage compared to static-field IMRT in head and neck malignancies [35]. This suggests that depending on clinical situation despite receiving effective treatment, patients could experience reduced side effects like xerostomia. Also, it is known that in comparison with IMRT treatment planning technique the continual rotation and radiation delivery of the unit (linear accelerator) shorten treatment times by half, especially irradiating tumour located in a pelvis region. This improves patient comfort and assures accuracy of the treatment by minimizing the possible internal organs changes and movements per time [16]. The dosimetry comparison shows [36] that VMAT consistently may result in lower doses to organs at risk, such as the femoral head, compared to IMRT. The dose-volume histograms DVH curves indicate that VMAT plans spare these structures more effectively, with smaller volume percentages receiving high doses as shown in (Fig. 6) [36]. This improved organ sparing and enabled more precise dose modulation. Several studies have reported that VMAT can effectively reduce the risk of late toxicities, such as osteonecrosis, without lowering target coverage. However, it is important to note that this is not always the case; in some treatment plans and localizations, IMRT can be equally optimized to achieve comparable or even superior sparing of organs at risk through careful planning and dose optimization [37]. Therefore, while many studies highlight the benefits of VMAT in minimizing normal tissue exposure, the actual dosimetry advantage can vary depending on the specific case and planning strategy [34].

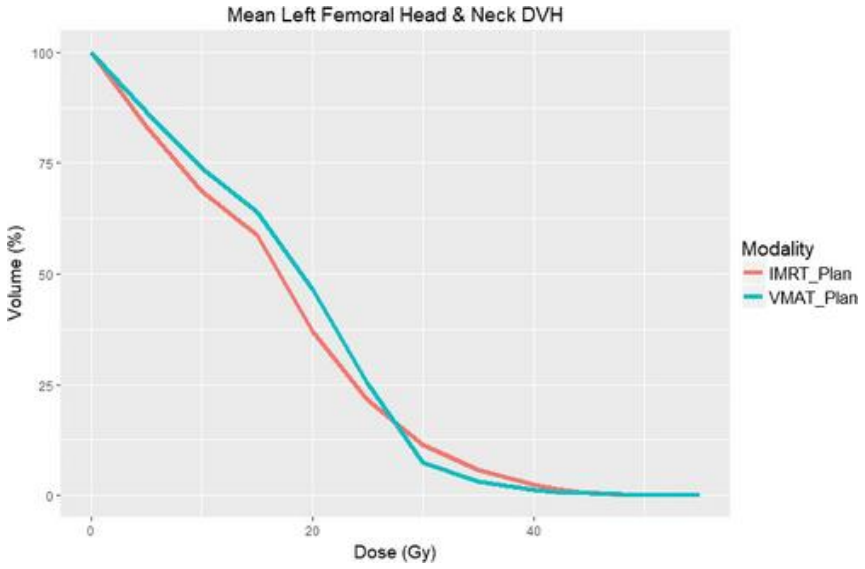

Fig. 6. Comparison of dose-volume histograms (DVH) for the left femoral head and neck in IMRT and VMAT plans [36]

Table 1. Comparison of IMRT and VMAT techniques in radiation therapy [31, 37]

Aspect	IMRT	VMAT
Beam modulation technique	Utilizes sliding window (dynamic) or step-and-shoot (static) methods with multi-leaf collimators (MLC) to modulate beam intensity.	Involves dynamic adjustment of gantry speed, dose rate, and MLC positions during arc rotation.
Dose distribution	Highly conformal, allows modulation of beam intensities to cover irregular tumour shapes.	Highly conformal, adjusts beam continuously in an arc pattern for precise targeting.
Treatment time	Generally, it is longer due to multiple beam angles and step & shoot technique, with an exception for bore type linear accelerator *Halcyon* (treatment time for IMRT and VMAT can be similar).	On the unit *Halcyon*, treatment time for IMRT and VMAT can be similar, dependent on unit used.
Number of beam angles	Utilizes multiple static angles.	Uses dynamic arcs, covering multiple angles within a single rotation.
Monitor units (MUs)	Generally, it requires more MUs than VMAT, leading to longer treatment times.	Typically, fewer MUs, reducing overall radiation exposure.
Secondary malignancy risk	Potential increase due to higher MUs and larger volume of irradiated tissue.	Comparative studies suggest similar or lower risks than IMRT.

Intensity-modulated radiation therapy (IMRT) and volumetric modulated arc therapy (VMAT) treatment planning techniques even mean an enhancement of the target conformity and led to minimization of the doses to organs at risk, however, studies [32] indicate that these techniques may result in elevated out-of-field doses.

1.4. Out-of-field Doses in Radiation Therapy

Out-of-field doses, which refer to unintended radiation exposure to tissues and organs outside the primary target/tumour volume, are an unavoidable consequence of external beam radiation therapy, which can be resulted by radiation scatter, leakage, and secondary particle production [38]. Although these doses are typically low compared to the prescribed tumour dose, their cumulative effect and the potential for long-term health consequences, such as risk of secondary cancer, raise significant concerns, especially when survival rate due to innovative treatment planning and delivery techniques increases [3]. Accurate determination of these doses is crucial for assessing and mitigating potential risks, using dose constraint for the organs at risk [39]. Radiotherapy treatment planning systems (TPSs) are not designed to perform calculations for doses outside the treatment field, and it is known that there are concerns regarding the precision of dose estimations provided by calculation algorithms of TPSs [38].

1.4.1. Evaluation of the Out-of-field Doses

Accurate determination of out-of-field doses is crucial step assessing the potential risks of secondary cancer induction and other side-effects [40]. Several methods are employed to estimate these doses, each with its own strengths and limitations Table 2.

Table 2. Comparison of methods for measuring out-of-field doses in radiation therapy [3, 41, 42]

Method	Description	Strengths	Limitations
Physical dosimetry	Radio-photoluminescent glass dosimeters (RPLGDs), thermoluminescent dosimeters (TLDs), diodes, and ionization chambers measure radiation exposure outside the treatment field.	High precision for specific measurements.	Limited measurement points; potential perturbation of radiation field.
Treatment planning systems	TPSs, such as *Eclipse* using anisotropic analytical algorithm (AAA)* and Acuros XB** algorithms, estimate dose distributions but may underestimate out-of-field doses due to simplified models.	Widely used and integrated into treatment workflows.	Inaccurate out-of-field estimates, as seen in studies showing up to 55 % underestimation.
Monte Carlo (MC) simulations	Considered the gold standard for calculating out-of-field doses, MC simulations accurately model radiation interactions but are computationally intensive.	High accuracy in predicting out-of-field doses.	Require detailed knowledge of treatment geometry and machine.

* The anisotropic analytical algorithm (AAA) is among the widely used algorithms in the *Eclipse* treatment planning system (Varian Medical Systems, Palo Alto, CA). By using several dose kernels to evaluate the dose contributions from different radiation sources inside a therapeutic beam, the AAA enhances upon conventional pencil beam techniques as a convolution/superposition-based technique. Although the AAA greatly improves dosage accuracy in modelling penumbra, low-dose zones, and field profiles (both symmetric and asymmetric), it has limits especially in places far from lung tissue interfaces, where systematic under-dosing may develop [43].

** *Acuros* XB dosage computation method for external beam therapy planning uses the linear Boltzmann transport equation (LBTE). This new method precisely determines the macroscopic behaviour of radiation particles, including electrons and neutrons, as they interact with materials. This approach enables exact dosage descriptions inside specified volumes, thereby improving the capacity of treatment planning systems such as VMAT and IMRT in providing efficient radiation therapy and so reducing the risk of problems [44].

Meta-analysis [45], demonstrated an association between out-of-field doses and subsequent cancer risk in childhood cancer survivors treated with radiotherapy. This demonstrates the significance of precise evaluation of unintended radiation outside the primary treatment volume, because even low doses to healthy tissues surrounding the tumour could contribute to long-term cancer risk. This implies that off-target radiation doses may increase the secondary cancer risk. In line with this [46] has suggested that intensity-modulated radiation therapy (IMRT), while improving target conformity, may also increase the risk of such radiation-induced secondary malignancies. This increased risk is because of the greater quantity of normal tissue that is irradiated to a low dose of radiation and a greater number of monitor units (MUs) used to deliver the treatment. They calculated that IMRT might raise the risk of secondary cancers 1.5 to 2 times the level in 3D plans, depending on the dose to nontarget tissues. Moreover, the ratio of average measured to prescribed doses across the TPS for an individual TPS (Fig. 7) demonstrates a systematic underestimation of out-of-field doses by TPS algorithm that points the necessity of dosimetry measurement in both therapeutic and risk assessment practices. These results underline the clinical relevance of the necessity of such dose verification, especially in paediatric and AYA patients, to allow long-term safety to be better estimated, and to drive evidence-based optimization of the RT planning [38].

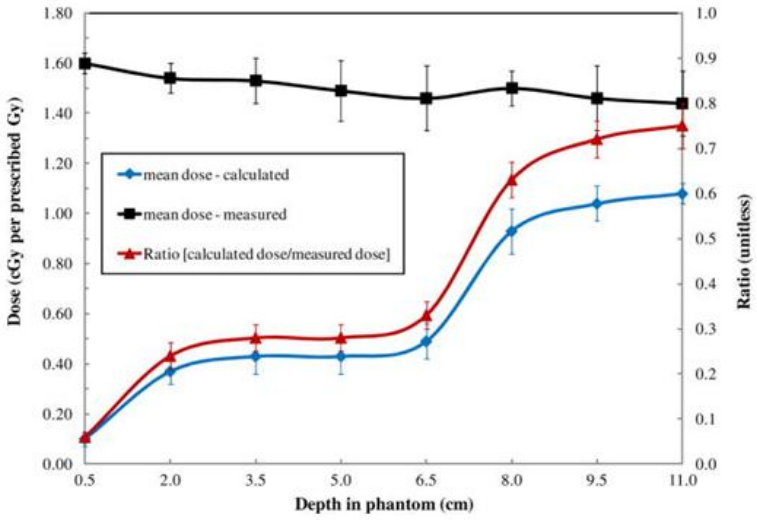

Fig. 7. Average absorbed doses measured and calculated at different depths in the phantom [38]

Notably, this underestimation was more pronounced at shallower depths compared to deeper situated tissues, potentially impacting the assessment of out-of-field doses induced risks and secondary cancer development [38].

1.4.2. Factors influencing out-of-field doses

The magnitude and spatial distribution of out-of-field radiation doses are influenced by several interrelated factors, including beam energy and modality, treatment field parameters, patient anatomy, and the dose calculation algorithm employed.

- **Energy and modality**. Higher photon energies, particularly those above 10 MV, tend to produce increased out-of-field doses due to enhanced photon penetration and the generation of secondary neutrons. Studies have shown that the use of 9 MV photon beams results in significantly higher peripheral doses compared to 6 MV beams at various tissue depths (1, 2, 3, and 5 cm) [47] (Fig. 8). While proton therapy offers superior dose conformity and lower integral dose compared to conventional photon therapy, it is not exempt from generating out-of-field doses. These arise primarily from nuclear interactions within patient tissues and beamline components, resulting in the production of secondary particles, including neutrons, which can deposit dose far from the treatment fields [48].
- **Field size and shape**. Larger field sizes and irregular or highly modulated field shapes are associated with increased scatter radiation, thereby raising out-of-field dose levels. Complex treatment techniques, such as IMRT and VMAT, often utilize multiple fields and dynamic beam modulation, which inherently increases the total monitor units (MUs) and contributes to greater peripheral dose deposition [49].
- **Anatomy and composition of the patient**. Individual anatomical variation, including patient size, body contour, and internal tissue composition also plays a significant role in the distribution of out-of-field doses. Larger patients tend to receive higher scattered doses due to greater internal scattering volumes, while tissue density differences (e.g., bone vs. soft tissue) can influence local dose deposition patterns [50].
- **Radiotherapy delivery system and dose calculation algorithm**. The type of linear accelerator and the algorithm used in the treatment planning system (TPS) critically influence the accuracy of out-of-field dose prediction. For instance, patients treated using 3D conformal radiotherapy (3D-CRT) with modern platforms like the Varian *Halcyon* system which employs flattening filter-

free (FFF) beams and an enclosed bore design have demonstrated improved sparing of tissues outside the primary field, particularly beyond 20 cm from the treatment edge in the cranial direction (Fig. 9) [48].

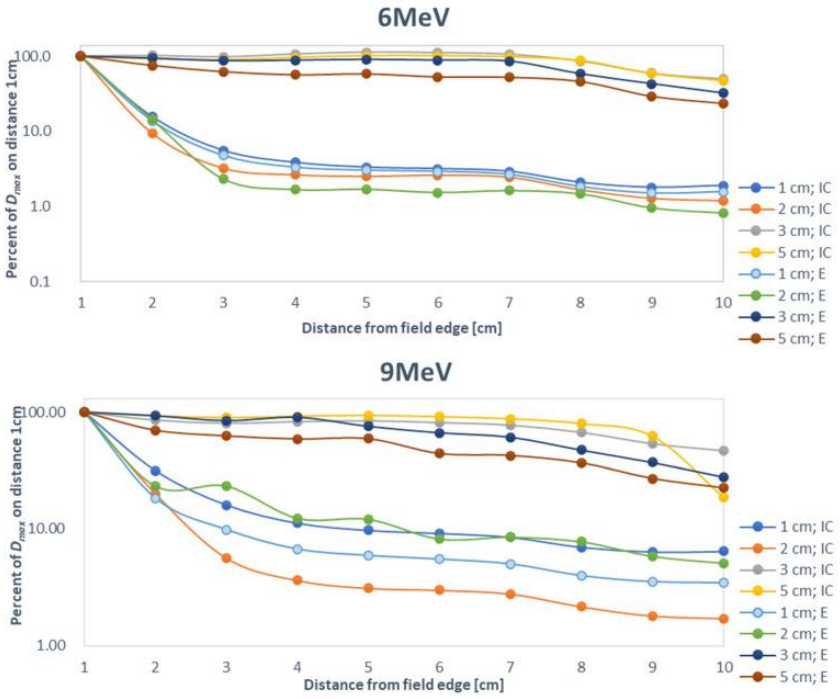

Fig. 8. Comparison of out-of-field doses at various electron beam energies (6 MeV and 9 MeV) [47]

Additionally, the accuracy of TPS dose prediction varies by algorithm. Studies have shown that both *Acuros* XB and the Anisotropic Analytical Algorithm (AAA) tend to underestimate out-of-field doses, particularly at distances ≥10 cm from the planning target volume (PTV) [43, 44].

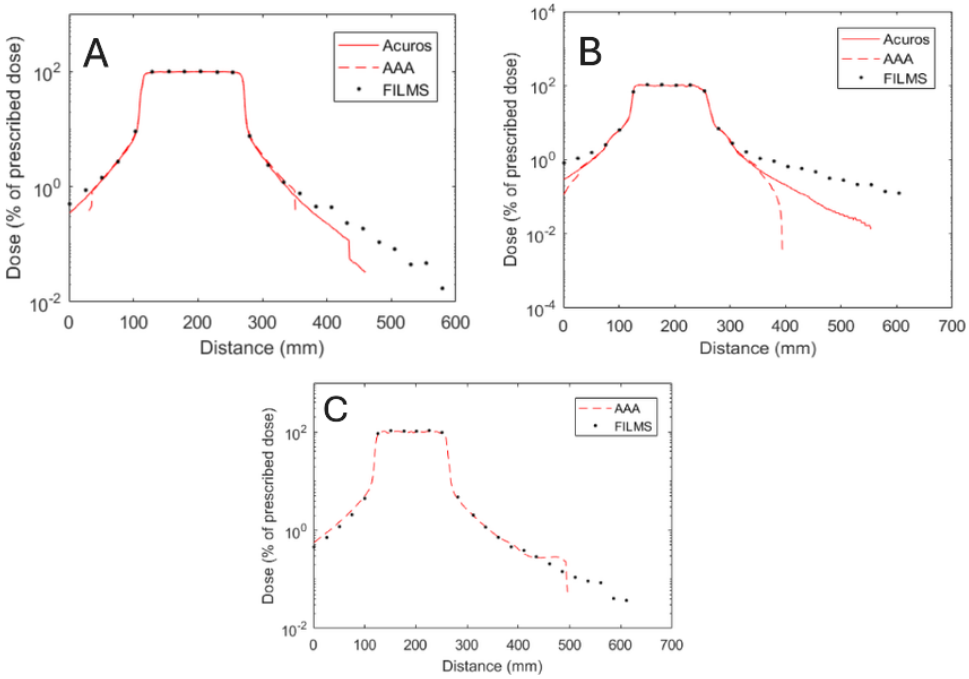

Fig. 9. Dosimetric validation: TPS-calculated vs. Radiochromic film measurements in a phantom. (A) 3D-CRT, (B) VMAT, (C) *Halcyon* [48]

Acuros XB models dose fall-off more gradually, while AAA typically predicts a steeper decline in dose with distance. This discrepancy is especially pronounced in volumetric modulated arc therapy (VMAT), where out-of-field dose modelling remains a known limitation of commercial TPSs [51].

1.5. Measurements of Out-of-field Doses

The precise evaluation of out-of-field absorbed doses is necessary for an accurate estimate of the risk of collateral exposure of healthy tissues as well as for an estimate of radiation-induced secondary malignancies. These measurements are affected by; the phantom type, the properties of the treatment beam and the method of dosimetry used [49]. In current external beam radiotherapy (EBRT), two typical dose estimation methods are employed: treatment planning system (TPS) dosimetry including Monte Carlo simulation, and physical dosimetry including experimental irradiation with dosimeter [41, 42]. Although TPS algorithms are well-validated in in-field regions, they are not specifically intended to predict dose deposition in the periphery. Such restriction commonly leads to considerable underestimation of out-of-field doses, especially when the distance from the planning target volume (PTV) increases over 10 cm. These disparities have been noted in several studies. For example, [38] have found that the TPS algorithms may underestimate the out-of-field doses by as much as 55% at a distance of about 11 cm compared to thermoluminescent dosimeter (TLD) measurements. Another study [52] found more variability, underestimate ranging from less than 100% to less than 14% and overestimates from less than 4 to 14%, depending on organ site and number of segments in the IMRT plan. Likewise, discrepancies of up to 100% of dose have been observed in clinical studies when comparing monte carlo simulations with TPS calculations based on superposition algorithms in peripheral organs [3].

Another study [42] have reported that using water phantom with thermoluminescent dosimeter (TLD) means coifs of were given flue days persist for there was. out-of-field IMRT doses were about 10–15% higher at the same distances. Studies on paediatric patients with child-sized phantoms demonstrated 1.5–2 times higher relative risks of secondary cancers relative to treatments in adults, highlighting the need to consider out-of-field doses in young patients [48].

Precise quantification of out-of-field doses in radiotherapy usually requires the use of dedicated dosimeters (e.g., TLDs, OSLDs and ionization chambers) and radiochromic films [53, 54]. All these devices bring specific benefits related to their sensitivity, spatial resolution, and ease of implementation to perform the full characterization of the low dose region far from the main treatment field.

1.6. Dosimetry in radiotherapy

Radiation dosimetry is a fundamental component of modern radiotherapy, essential for evaluating dose-response relationships and ensuring the safety and effectiveness of treatment [55]. Accurate dose estimation is crucial not only within the treatment field "in-field" but also near its margins "near-field" and in anatomically distant regions ("out-of-field") that may still receive unintended radiation. Out-of-field radiation doses tend to decrease significantly with distance from the primary beam and primarily result from three sources: (1) scatter radiation generated within the patient's body, (2) scatter from the linear accelerator (LINAC) head, and (3) radiation leakage through LINAC shielding [47].

1.6.1. Ionization Chambers Dosimetry

Ionization chambers are among the most established and widely used instruments in radiotherapy dosimetry. They provide highly accurate, real-time measurements of ionizing radiation, making them indispensable for absolute dose calibration, quality assurance, and in vivo and phantom-based measurements [56].

These chambers operate by collecting the charge produced when ionizing radiation interacts with gas molecules typically air, argon, or nitrogen—inside a sealed cylindrical volume (Fig. 10) The resulting ion pairs are attracted to electrodes under an applied electric field, generating a current directly proportional to the absorbed dose. This current is read by an electrometer and converted into dose values expressed in gray (Gy) [54, 56]. Due to their excellent reproducibility, energy independence (when properly calibrated), and sensitivity, ionization chambers are often considered the gold standard for reference dosimetry and are recommended by protocols such as IAEA TRS-398 and AAPM TG-51 [57].

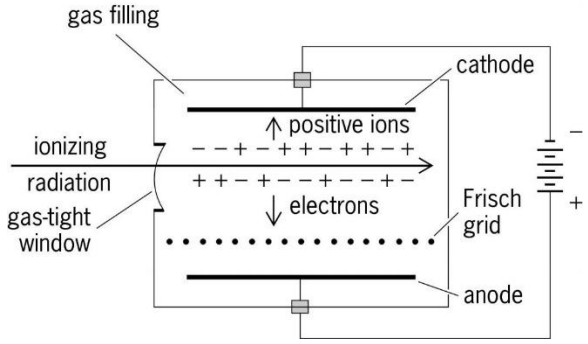

Fig. 10. Schematic representation of ionization chamber [56]

Due to their high precision, linearity, and stability, ionization chambers are particularly effective for point dose measurements in low-dose regions, making them suitable for quantifying out-of-field doses when properly calibrated [58]. Their relatively low energy dependence and well-established correction factors allow for accurate assessment, even at peripheral distances from the treatment volume [59].

Importantly, ionization chambers are well suited for out-of-field dose measurements, where radiation levels are relatively low and often fall below the reliable detection thresholds of other dosimeters. Several studies have demonstrated their effectiveness in this context. For example, Howell et al. [38] used ion chambers to measure peripheral doses in an anthropomorphic phantom and found that treatment planning systems (TPS), particularly those relying on simplified scatter models, underestimated out-of-field doses by up to 50%, especially at distances greater than 10 cm from the treatment field. Similarly, Kry et al. [60] used ionization chambers to measure photon and neutron dose equivalents in patients during IMRT, showing significant differences between measured and TPS dose values.

These results highlight that ionization chambers are useful, accurate tools to measure out-of-field exposure especially in the experimental verification of dose calculation algorithms and in crital organs' dose assessment lying outside the high-dose area. Their accuracy at low dose levels and the ease of traceable calibration have made them essential tools in the quality assurance of radiotherapy, peripheral dose audit, and secondary cancer risk modelling.

1.6.2. Thermoluminescent dosimeters (TLDs)

TLDs are employed widely in radiotherapy dosimetry because they are small, reusable and can faithfully measure the accumulated radiation dose with time. Solids state detectors work by absorbing the radiation energy exciting electrons to higher energy levels in a crystal lattice, typically lithi um fluoride (LiF). These electrons are then localized on defects or impurities in the crystal structure. During the readout cycle, the TLD material is heated, the trapped electrons are stimulated to return to their base state relaxation and release energy in the form of visible light. Intensity of the light emitted is directly proportional to the absorbed dose of radiation and is detected by a photomultiplier tube or similar device (Fig. 11) [53].

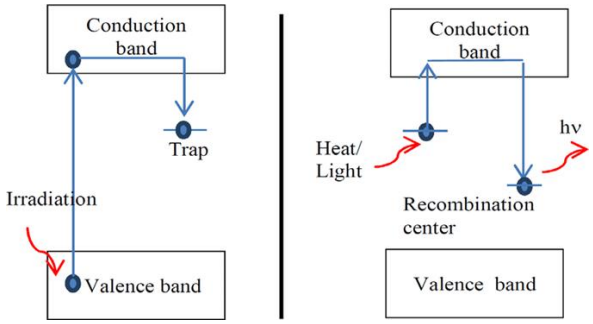

Fig. 11. Fundamental concepts of thermoluminescent dosimeters (TLD) [61]

TLDs are especially useful for out-of-field dose measurements with low and non-uniform radiation levels. Due to their high sensitivity, low-cost and large number available, they can detect low-dose radiation far away from treatment field, being especially useful for a study of scattered dose to critical organs. TLDs were used together with diode detectors in a study by Kinhikar et al [62], to measure peripheral doses during intensity-modulated radiation therapy (IMRT) delivered with both conventional linear accelerators and tomotherapy units. Results showed the TLD to be a reliable instrument for measuring doses up to 25 cm from the field edge, an indication of its ability to measure low-dose regions peripheral to the field. The study also reported peripheral doses tended to be lower with tomotherapy versus standard linear accelerators and underscores the significance of precise dosimetry when comparing treatment approaches [62]. Furthermore, Mazonakis et al [42], used TLDs with anthropomorphic phantoms to measure peripheral dose distributions in breast radiotherapy. Their work confirmed the dosimetry correctness of TLD for low dose radiation in the peripheral tissues due to the agreement between TLD measurements and Monte Carlo calculations.

In order to be used in clinical and research settings, TLD measurements need to be accurately calibrated and placed to ensure minimal variation. Environmental influences such as scatter radiation and angular dependence have also to be accounted for. Correctly used, TLD measurements provide a reliable and consistent means of quantifying dose distributions in regions beyond the primary treatment field.

1.6.3. Optically Stimulated Luminescence Dosimeters (OSLDs)

Optically Stimulated Luminescence Dosimeters (OSLDs) are increasingly useful in radiotherapy dosimetry for the evaluation of out-of-field doses. The dosimeters are based on the concept that certain substances, for example beryllium oxide (BeO), trap energy after exposure of ionizing radiation. Upon irradiation with light, they release this energy as luminescence intensity, related to the absorbed dose. By comparison OSLD advantages are high sensitivity, reusability and the

potential for providing accurate dose in low dose region [63]. In a study by Quan et al [64], used OSLDs to assess out-of-field doses generated by a 1.5 T MR-Linac. The study showed that OSLDs could accurately measure surface and internal doses in anthropomorphic phantoms and highlighted a significant increase in the MR-Linac out of field doses relative to a standard linear accelerator. This work highlights the applicability of OSLDs to the estimation of peripheral doses, particularly in modern radiation therapy facilities, where the presence of magnetic fields may impact the dose delivery. Furthermore, Kenzevic et al [63] compared OSLDs with ionization chambers for the measurement of out-of-field doses in IMRT by Kenzevic et al. Results: The results have shown that OSLDs make accurate measurements, which can be used as an alternative to ionization chamber measurements in low-dose region outside the primary treatment volume.

These results demonstrate the importance of OSLDs in dosimetry for out-of-field doses, leading to better treatment planning and risk estimation in radiotherapy.

1.6.4. Radiochromic Films Dosimetry

The Gafchromic™ EBT series is a type of radiochromic film and its characteristic features for dosimetry in radiotherapy include high spatial resolution, near-tissue equivalence and 'self-developing' nature. Those films have exhibited a colour change when exposed to ionizing radiation, which can be used to make accurate two-dimensional dose distribution measurements without chemical processing [65]. Radiochromic films have been found particularly useful in out-of-field dose measurements. Their low-dose-region sensitivity allows accurate visualization of peripheral doses, which is important for evaluation of exposure of the nearby healthy tissue outside the treatment field. A work by Colnot et al [48], who investigated the out-of-field doses from three radiotherapy techniques, 3DCRT, VMAT and tomotherapy, using Gafchromic™ EBT3 films placed in a paediatric anthropomorphic phantom, showed a significant dependence on the used techniques and that tomotherapy gave slightly the highest peripheral dose. This study highlights the significance of choice of the technique in limiting the unintended radiation exposure of non-target tissues.

Further research by Piotrowski et al [66] Dosages in different organs were measured in a phantom model using radiochromic films. Peripheral organ doses such as intestines and lungs had measurable doses, and biological response was expected in the periphery as well as in the primary treatment region. These studies illustrate the importance of using radiochromic films for accurate out-of-field dosimetry which is used for the correlation of treatment planning and evaluation of risk in order to improve patient safety in radiotherapy.

1.7. The Importance of Sparing Organs at Risks in Head and Neck Cancer Radiotherapy

The complex anatomy of the head and neck (HN) region calls for careful evaluation of organs at risk (OARs) during the radiotherapy process (Fig. 12) [67]. OARs, near target volume/planning target volume (PTV), are quite vulnerable to radiation-induced damage, which can greatly compromise a patient’s quality of life. It is known that the parotid, submandibular, and sublingual glands are related to saliva generation. For this reason, ionising radiation induced damage to the mentioned glands can cause xerostomia [68], a common and crippling condition that seriously compromises patient’s well-being. Therefore, sparing of the parotid glands is a crucial step in radiotherapy planning process, keeping the average radiation dose below 26 Gy, which can be helpful maintaining salivary function [25, 28].

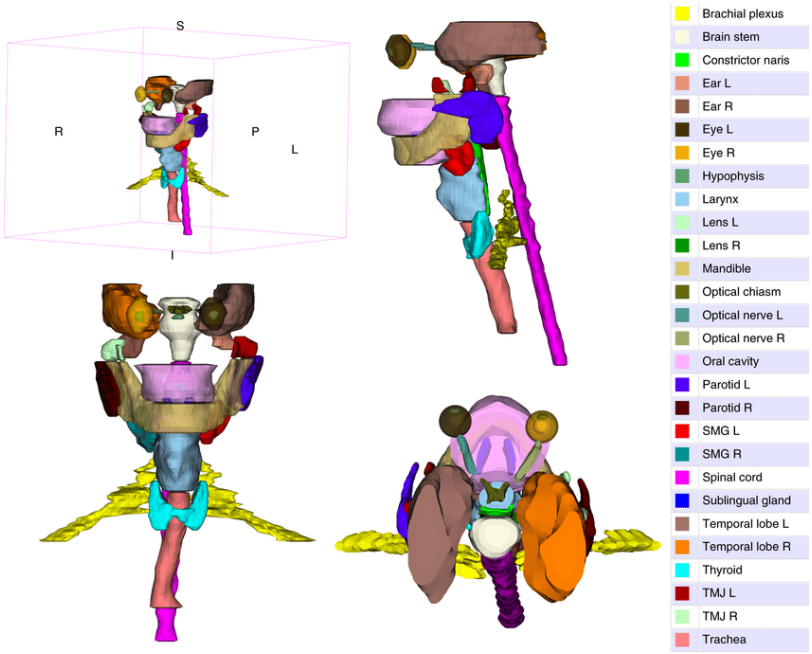

Fig. 12. Organs at risk in the head and neck region [69]

Beyond the salivary glands, the spinal cord and brainstem are also critical structures with low tolerance to radiation. According to Kirkpatrick et al. % [24, 28], the risk of myelopathy increases markedly when radiation doses to the spinal cord exceed 50 Gy delivered in 2 Gy fractions. Therefore, it is essential to delineate the spinal cord precisely and adhere to recommended dose constraints, usually keeping the maximum dose below 45 Gy to avoid this serious and potentially irreversible complication [70]. In general, meticulous sparing of OARs help minimize both acute and chronic toxicities associated with radiotherapy. Acute side effects, such as mucositis, skin irritation, and fatigue, can significantly affect patients' daily lives, sometimes necessitating treatment interruptions and influence treatment compliance. On the contrary, late effects, including fibrosis, necrosis, and secondary malignancies, may emerge months or even years after treatment, further affecting long-term quality of life [71]. By targeting radiation more precisely to avoid OARs and adhering to established dose constraints, clinicians can mitigate these risks, ultimately leading to better long-term health outcomes and improved conditions of life for HNC patients [69].

1.8. Secondary Cancer Risk in Head and Neck Cancer

While radiotherapy significantly enhances survival rates in mucosal cancer of the head and neck, with overall 5-year overall survival rates estimated at 65 % (SEER data, 2008-2014), the long-term risk of second primary cancers (SPCs) remains a pressing concern [72]. As the risk of recurrence of head and neck squamous cell carcinoma (HNSCC) decreases over time, survival care increasingly prioritizes the management of long-term therapy effects and early detection of SPC [72]. First of all, HNC survivors are particularly prone to developing secondary malignancies in the lung, oesophagus, and additional head and neck site, suggesting shared etiological factors and/or the effects of field cancerization. These SPCs often share common risk factors with the original HNC, including persistent tobacco and alcohol use, highlighting the importance of comprehensive lifestyle interventions, such as smoking cessation and alcohol moderation programs, for this population [6]. Data from GLOBOCAN [73] indicate that incidence rates of secondary carcinomas vary by head and neck location, ranging from 1.2 per 100,000 in the nasopharynx to 4.3 per 100,000 in the oral cavity, reflecting differences in exposure to carcinogens and/or variations in genetic susceptibility. In

addition, HNC constitutes 4.58 % of all cancer-related deaths worldwide, highlighting the significant burden of this disease [74]. As shown in (Fig. 13), head and neck sites account for the largest proportion of second primary cancers, reinforcing the high vulnerability of this group to SPCs. The increasing number of survivors of HNSCC, a testament to advances in early detection and treatment, increases the need to address long-term risks, particularly the development of secondary primary malignant neoplasms (SPMN). These patients face an elevated risk of SPMN, with annual incidence rates ranging from 3 % to 7 % and a cumulative risk of 36 % over 20 years. Alarmingly, SPMNs contribute to approximately one-third of all deaths in patients with HNC, often exceeding mortality from metastatic disease and serving as a crucial factor in long-term survival [75]. This high mortality rate underscores the need for improved strategies for the prevention and detection of SPC in HNC survivors.

Although radiotherapy is vital for controlling primary tumours, it can also paradoxically induce SPCs by damaging DNA in healthy surrounding tissues. Factors that influence this risk include the total radiation dose delivered, the fractionation schedule used, and the volume of tissue irradiated. A significant and often unavoidable concern is exposure of healthy tissues to radiation doses out of the field during treatment. Although contemporary methodologies, such as intensity-modulated radiation therapy (IMRT) and volumetric modulated arc therapy (VMAT), aim to minimize exposure to organs at risk, low doses of radiation can still reach distant tissues, potentially elevating the long-term risk of secondary cancers [5]. Moreover, new studies show that personal genetic characteristics, including variants of DNA repair genes, may also modify one' s susceptibility to radiation-irradiation-induced second cancers that underlie the difficulty in predicting and reducing SPC risk [76].

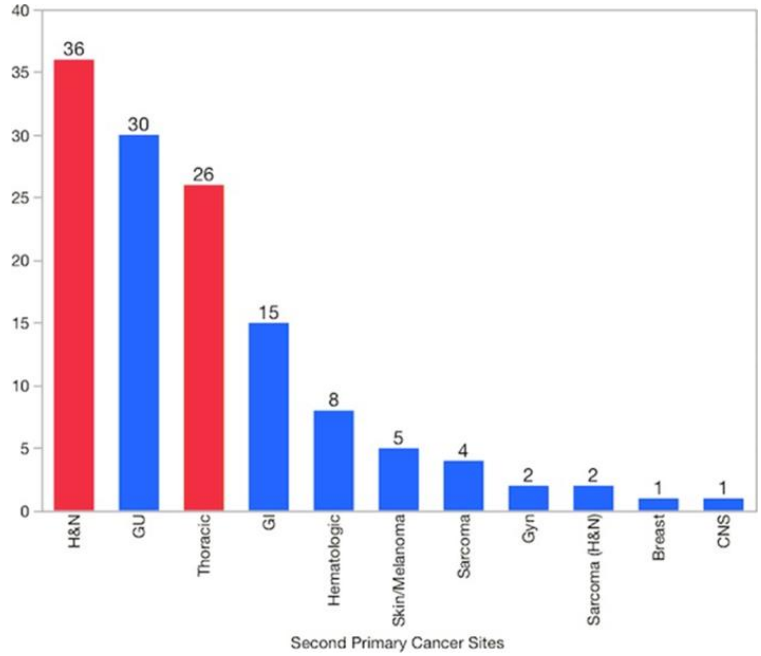

Fig. 13. Locations and occurrences of second primary cancers [72]

This observation implies that a personalized risk assessment including dosimetric and genetic factors is important for the optimization of the treatment approaches to not only reduce the normal tissue burden but also to minimize the long-term effects of radiation therapy.

1.9. Biologic effects of ionizing radiation (BEIR) VII model

The BEIR VII model (Biologic Effects of Ionizing Radiation VII) for predicting health risks from exposure to low levels of ionizing radiation, developed by the National Research Council of the National Academies, has played a major role among radiation protection professionals in setting policies. Released in 2006, the model describes primarily the association between low dose ionizing radiation and the risk of developing cancer and is based on the evaluation of extensive epidemiological studies of A-bomb survivors, occupational and medical exposures [77]. The committee for the BEIR VII modelled total risk, which accounts for variation in risk factors and that is intended to unify excess relative risk (ERR) and excess absolute risk models (EAR) by applying each where the uncertainties in estimating cancer risk from radiation were greatest [42]. The dose calculations are based on the radiation dosimetry protocol described in the BEIR VII model, and the EAR and ERR are estimated with the equations:

$$EAR = \beta_s D\ EXP(\gamma e^*)(\frac{a}{60})^n \quad (1)$$

$$ERR = \beta_s D\ EXP(\gamma e^*)(\frac{a}{60})^n \quad (2)$$

Where *D* is the dose, *e* represents the age of the individual at the time of exposure, measured in years (e^* is (e – 30) / 10 for e < 30 and zero for e <30), and a denotes the age obtained of the individual, measured in years [42]. In this approach, the secondary cancer risk is proportional to the organ dose [78]. While widely used, the BEIR VII model is not without limitations, and has been the subject of continued disagreements and criticisms about its assumptions and generalization across exposure scenarios. Central to the debate is a theory called the linear no-threshold (LNT) model, which posits that any dose of radiation, no matter how small, has the potential to cause cancer. Some of the debate concerns whether or not LNT overestimates, the risk at very low doses or underestimates, the risk because of nontargeted effects of the radiation, including what could be termed genomic impostures and bystander effects [79].

Furthermore, the model makes extensive use of atomic bomb survivor data, in which individuals were exposed acutely at relatively high doses, and this raises a question as to whether to what extent such assumptions are applicable to chronic low-dose exposures typically encountered in occupational and medical contexts [78]. In the current scenario of HNC radiotherapy, the application of the BEIR VII model may also be further restricted by the complexity of the head and neck anatomy, the diversity of HNC sub-types (HPV-positive vs. HPV-negative) and usage of multi-modality treatments [72]. Although the BEIR VII model serves as a useful overall framework for estimation of radiation-induced cancer risk, there is increasing consensus that more personalized risk prediction models that consider other host factors (sex, age, smoking history, alcohol intake, genetic susceptibility [e.g., DNA repair capacity], and detailed dosimetry that would include accurate estimates of out-of-field doses) are required [48]. These individualized dosimetry approaches, accounting for age- and gender-based anatomical and physiological variation are important factors in minimizing out-of-field doses and thus potentially reducing the long-term risk of secondary cancers in HNC survivors.

1.10. Gender-related factors in head and neck cancer

1.10.1. Incidence and prevalence

Head and neck cancer (HNC) has a profound gender disparity and males have a far greater incidence of the disease than females. The male to female ratio is usually between 2:1 to 4:1 (Fig. 14), although this ratio can vary depending on the specific anatomical site and geographical region.

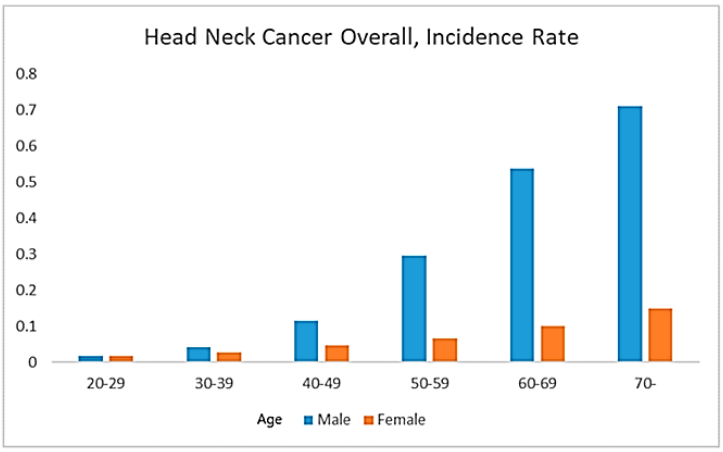

Fig. 14. Head and neck incidence rate [80]

This gender discrepancy has been addressed in numerous epidemiological studies and may reflect the effects of certain biological and lifestyle-related factors that are more prevalent in men [7]. Although behavioural risks (such as tobacco and alcohol use) contribute to HNC in both sexes, recent meta-analyses [80] demonstrated that the sex difference remains even after adjusting for these factors, and hormonal, inherited susceptibility, or immune response disparities may also contribute.

1.10.2. Differences in organ doses

The influence of gender is also apparent in radiation therapy, where anatomical and physiological differences may result in differences in organ doses. It has been demonstrated that the distribution of the dose during radiotherapy for HNC could differ according to the gender of the patient. For instance, a systematic review by Zhang et al. [41] concluded that the doses delivered to certain critical organs, including the parotid and thyroid glands, to males were significantly higher than those to females (mean difference: 2.3 Gy, $P<0.001$). There may be differences in neck anatomy (muscle mass, fat distribution), and/or the treated volume, that could account for these dose differences. Differences in organ doses may have implications for both treatment response impacting tumour control and late toxicity affecting salivary function, thyroid function and the incidence of secondary malignancies [41]. Thus, there may be a role for gender-tailored treatment planning strategies to improve response rates and reduce toxicity in male and female HNC patients.

1.11. Age-related factors in head and neck cancer

Age affects diagnosis, therapeutic strategies, tolerability to treatments and survival in head and neck cancer (HNC) patients. With increasing age among the population, it is more important to understand how different age-related factors affect disease and treatment effects [81]. This section investigates the impact of age on treatment workup and tolerance and age and its relationship with organ doses in HNC treated patients undergoing radiotherapy.

1.11.1. Influence of age on treatment approaches

Management of HNC in the elderly is challenging and age-related aspects should be included in therapeutic decision making. A review from Smith et al. [2], (Fig. 15) showed that older HNC patients (65 years) experienced 1.5 times elevated incidence of severe treatment-related toxicities (grades 3-4) compare to their younger counterparts (OR=1.53, 95% CI: 1.28-1.82, p<0.001).

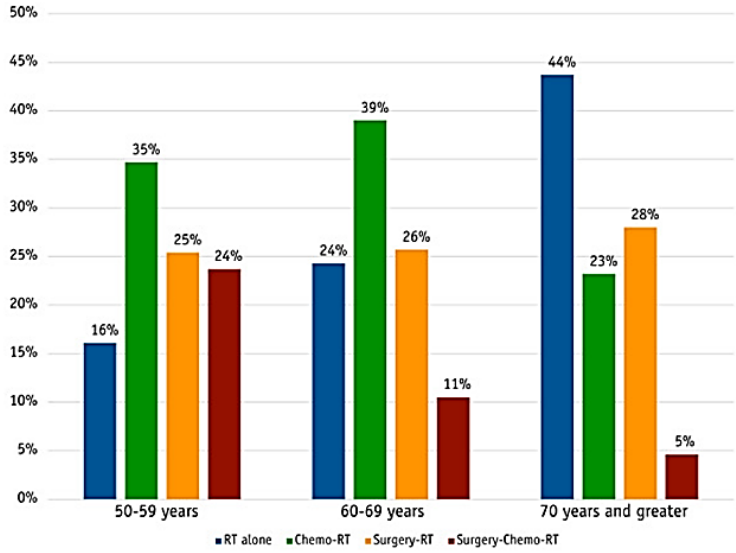

Fig. 15. Age and treatment approaches in head and neck cancer [82]

These results stress the importance of age-specific treatment options such as dose adaptation, accelerated radiation therapy fractionation schedules or unimodal modalities. A multidisciplinary approach is often recommended to aid in the development of individualized care plans to meet the elderly patients' holistic health needs [81].

1.11.2. Age and tolerance to treatment

Elder patients are more susceptible to chemotherapy and radiotherapy adverse events. For instance, a study by Garcia et al. [83] also found that individuals with HNC aged over 70 presented a 40 % greater chance of developing grade 3 or greater mucositis as compared to those under age 60 years (RR 1.40, 95 % CI: 1.25-1.57, p S <0.001). Hence, the hip-preserving treatment of these age-dependent conditions may also change, and differences in tolerability of treatment can be due to age-related alterations in body composition and organ function, which have an impact on pharmacokinetics and may need dose adaptation or another therapeutic approach [84].

1.11.3. Correlation between age and organ doses

Studies have reported strong association between age and radiation dose exposure to organs at risk (OAR) in radiation therapy. A dosimetry investigation of Wang et al. [7], showed older patients (i.e.>65 years) received 12% more doses to the parotids than younger patients (p=0.003). This difference was explained by age-related changes of the neck's anatomy (increased adipose tissue) and of muscle mass that might modify the spatial relations between tumour and adjacent organs. Furthermore, to support this, a comprehensive research made by Rodriguez et al. [9], Patients were also at least 70 years old and they achieved a higher mean maximum spinal cord dose 2.5 Gy higher than the younger than 50 years old patients (p<0.001; 95% CI: 1.8 & 3.2 Gy); age was an independent

predictor of spinal cord dose in a group of 500 HNC patients treated with intensity modulated radiation (IMRT).

These findings underscore the importance of incorporating age-specific considerations to treatment planning to mitigate the development of radiation effects of treatment. Late sequelae, such as xerostomia and osteoradionecrosis, occurring in the more elderly patients and those who have had a higher organ dosage also have been reported in long-term follow-up studies. For example, a retrospective study over 10 years by Thompson et al. [81] reported that HNC survivors aged 60+ y at the time of treatment, they were 1.8 times more likely to have grade 2 or worse late xerostomia (HR: 1.8, 95% CI: 1.4–2.3, $p<0.001$) than their younger counterparts (<50 years). This underscores the necessity of customized treatment strategies taking into account age-related anatomical and physiological alterations to minimize toxicity and optimize outcomes in elderly HNC patients.

1.12. Summary of Literature review

While many studies have examined various aspects of the radiotherapy for HNC, such as treatment modalities, dosimetric optimization, and toxicity control, there are several notable knowledge gaps regarding long-term risks of radiation exposure. Specifically, out-of-field doses are not understood in well detail and there is a limited understanding on the effect of patient specific factors such as gender and age with respect to risk of secondary cancer [85, 86]. These shortcomings diminish our ability to accurately predict and minimize the risk of secondary cancer and other late effects in the cured HNC population. Closing these gaps is key to better long-term outcomes in such patients. The following specific gaps warrant further research:

- The gender-specific anatomical and physiological differences contributing to modulated outside-of-field dose distribution and consequent cancer risk are not well characterized by existing studies. Differences in neck anatomy and hormonal status, for example, would result in varying radiation exposure and sensitivity [87].

- Also, of interest that warrants further research is the effect of age on radiation sensitivity and risk of late effects. Given that age-related alteration of DNA repair pathways, immune system, and tissue homeostasis can contribute to increased susceptibility of older patients to radiation damage, older patients may be rather sensitive to radiation exposure. However, only a limited number of studies have specifically investigated whether age impacts out-of-field dose distributions and the associated secondary-cancer risks in HNC survivors. This makes it difficult to tailor therapy plans to minimize late effects in elderly patients.

- While the increase in the out-of-field doses associated with IMRT and VMAT versus 3D-CRT have been documented in the literature [31], detailed data for the specific doses deposited in specific organs at risk (OARs) outside of the primary treatment volume are not currently available [88]. For newer techniques, such as adaptive radiotherapy and proton therapy, where the combined impact of dose conformity and out-of-field exposure requires further investigation, this is particularly the case. Furthermore, more complete characterization of out-of-field dose distributions using state-of-the-art measurement techniques, such as Monte Carlo simulations and in vivo dosimetry, is needed to verify TPS calculations and thus improve dose estimate. This lack of knowledge is a barrier to a precise evaluation of the risk and to personalized therapeutic decision-making.

Filling these voids in knowledge are critical for enhancing HNC survivors' long-term outcomes. The current study aims to address these limitations by considering out-of-field exposures, gender-specific differences, changes with age, personalized risk estimation, and the biological mechanisms. This may lead to more rational strategies for avoidance of additional late complications and secondary malignancy in this vulnerable patient population.

2. Materials and methods

Research of this study was performed at the Hospital of Lithuanian University of Health Sciences Kaunas Clinics, Oncology Hospital. Patient data were collected, and the main measurements of out-of-field doses based on anthropomorphic phantom *SHANE* were performed using Varian medical linear accelerator *Halcyon*.

2.1. Patient Cohort

The patient cohort consisted of 118 individuals diagnosed with head and neck cancer, comprising 21 females and 97 males, aged between 40 and 80 years. All the data were collected per 3 years between January 2022 and February 2025 (Appendix 1). Initially, 210 patients were observed during the mentioned period, but the final analysis included only 118 patients due to the handling of missing values and strict criteria for the statistical evaluation. The study also excluded patients who were older than 80 years at the time of radiotherapy. The dataset involved vital demographic and clinical variables such as patient age, gender, and cancer location. The treatment details included the total amount of radiation given (in Gy), the amount of radiation per session, and the specific radiation doses received by tissues and organs like the oesophagus, spinal cord, left and right parotid glands, parotids, left and right submandibular glands, and larynx. Additionally, clinical staging and tumour characteristics (T, N, M classification) were documented. All the cases received daily kV cone beam computed tomography (kV-CBCT) as the linear accelerator *Halcyon* is a 100 % image-guided radiation therapy (IGRT) system.

2.2. Linear Accelerator *Halcyon*

The linear accelerator *Halcyon* (Varian Medical Systems, Palo Alto, CA) was used for the head and neck cancer cases irradiation. This system emits a maximum of 6 MeV energy and forms flattening filter-free (FFF) photon beams. The dual-layer multi-leaf collimator (MLC) of the *Halcyon*, with a 1 cm leaf width at isocentre, is a key feature that enables precise beam shaping and accurate delivery of radiation to the target volumes, thereby contributing to improved sparing of adjacent organs at risk. Treatments were administered at a dose rate of 800 MU/min. An accurate patient and/or phantom positioning based on lasers formed (virtual isocentre) (Fig. 16) was ensured using integrated kV imaging system, capable of performing daily cone-beam computed tomography (CBCT) [89].

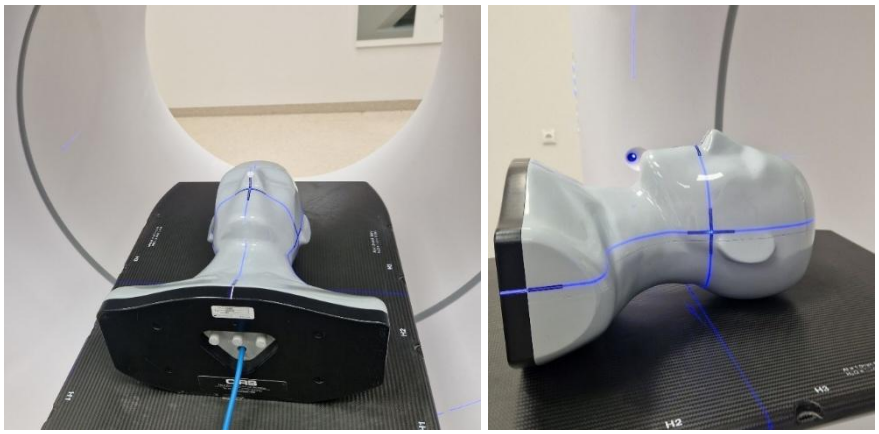

Fig. 16. Laser beam alignment in the linear accelerator *Halcyon* system with the phantom *SHANE*

2.3. Radiation Treatment Planning

Radiation treatment planning for HNC cases was performed using the treatment planning system *Eclipse* (Varian Medical Systems, Palo Alto, CA). Radiation oncologists delineated targets (the gross tumour volume (GTV), clinical target volume (CTV), and planning target volume (PTV)) and organs at risk (OARs) based on computed tomography (CT) images. Two advanced techniques for planning radiation treatments were employed: intensity-modulated radiation therapy (IMRT) and volumetric-modulated arc therapy (VMAT). IMRT and VMAT treatment planning techniques are inverse treatment planning modes, which are usually planned using maximum 6 MeV X-ray photon energy. The dose distributions were optimized based on anatomical considerations to optimize target coverage while sparing OARs. Dose constraints for OARs were summarized in Table 3.

Table 3. Dose constraints for organs at risk [90]

Organ at risk	Dose limitations, Gy
Oesophagus	*Dmean** < 30
Submandibular gland (left *or* right)	*Dmean* ≤ 35
Larynx	*Dmean* < 40
Oral cavity	Dmean ≤ 30
Parotid gland (left *or* right)	Dmean < 20
Both parotid glands (left *and* right)	*Dmean* ≤ 25
Spinal cord	*Dmax** ≤ 45
Brainstem	*Dmax* < 54
Thyroid	*Dmean* ≤ 40

**Dmean* – mean dose to the organ, *Dmax* – maximum dose to the organ.

Typically, the prescribed dose to the primary tumour and involved lymph nodes is 70 Gy, delivered in 35 fractions. However, in certain cases, the prescribed dose was reduced, ranging from 50 Gy to 70 Gy, depending on a certain clinical situation. Two sequential boost volumes were implemented, receiving prescribed total doses of 60 Gy and 70 Gy, respectively.

Treatment plans planned using the IMRT technique were based on specific angles (0°, 45°, 90°, 135°, 180°, 225°, 270°, 315°) and modulated intensity per irradiation field/beam, while VMAT plans were created using 2 or 3 full arcs (from 179° to 181° counter clockwise); in some specific cases, 2 or 3 partial arc strategies were used, depending on the patient's anatomy and tumour location (Fig. 17).

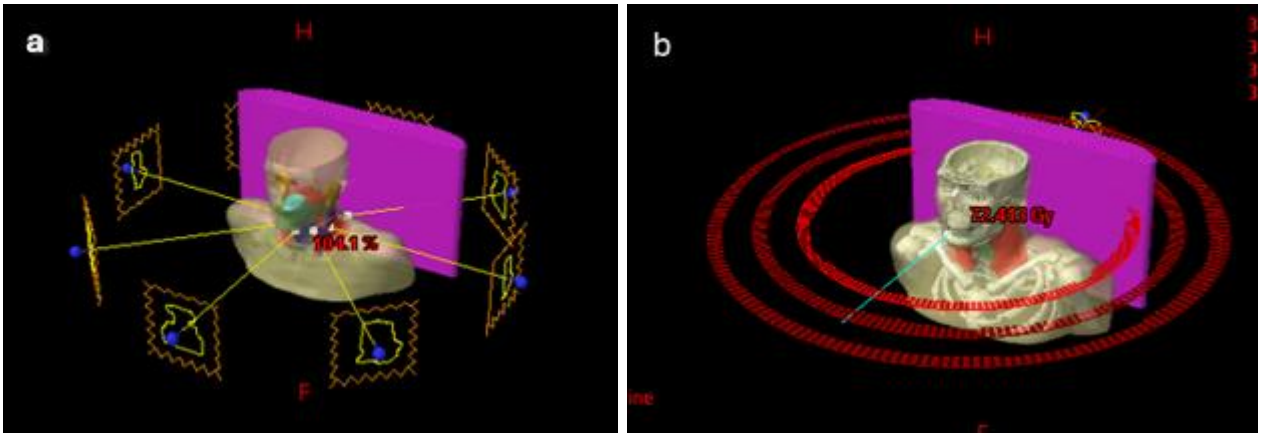

Fig. 17. Visualization of treatment planning techniques in Eclipse TPS: (a) IMRT plan, (b) VMAT plan

The dose calculation for both the IMRT and VMAT techniques were performed using two distinct algorithms within the treatment planning system *Eclipse*: The Anisotropic Analytical Algorithm (AAA) and the *Acuros* XB algorithm, trying to evaluate dose calculation models influence for the out-of-field doses measurements.

2.4. Measurements of Out-of-field Doses

To effectively replicate the intricate anatomical structure of the head and neck region for out-of-field doses assessment, this study employed the anthropomorphic phantom *Shane* (Shoulders Head and Neck End-to-End, CIRS, Norfolk, VA) [91]. The phantom *Shane*, which is based on the CIRS Model 038 verification phantom, provides a detailed model of the head and neck that is important for additional checking treatment plans and how they are carried out. This phantom was developed by the International Atomic Energy Agency (IAEA) [92] to support dosimetry audits in head and neck cancer radiotherapy.

This phantom is specifically designed to assess the entire radiotherapy process, encompassing image acquisition, treatment planning, and dose verification. Its construction closely mimics the complex anatomical features of the human head and neck, utilizing materials with densities similar to actual tissues, including soft tissue, muscle, bone, and teeth (Fig. 18). This design ensures that ionizing radiation interaction with the phantom closely resembles those that occur in real patients.

Moreover, the phantom can be disassembled to allow for dosimetry, gafchromic film insertion and features four hollow cylindrical channels that enable the placement of the cylindrical ionization chamber for measuring absorbed dose in the specific anatomical regions [93].

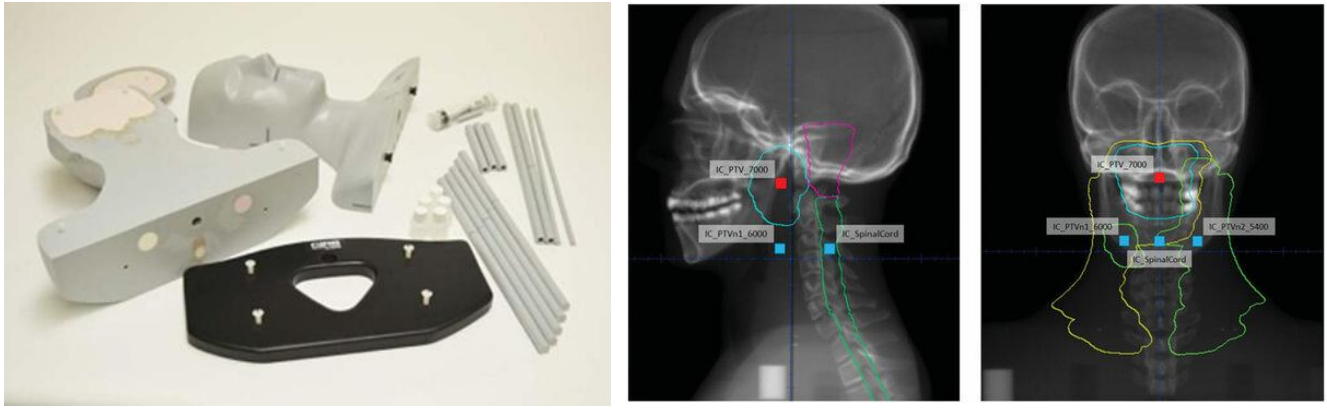

Fig. 18. Anthropomorphic phantom *Shane* [93] and CT images of the phantom [36]

Irradiation procedure was performed imitating HNC case standard procedure following recommended IAEA protocol [94]. The plan was planned with the treatment planning system *Eclipse* utilizing a simultaneous integrated boost (SIB). Three different PTVs (PTV_7000, PTVn1_6000, and PTVn2_5400) were defined, with the prescribed doses corresponding to 70 Gy, 60 Gy, and 54 Gy, respectively, delivered in a total of 35 fractions. Intensity modulated radiotherapy (IMRT) was used with beam angles of 0°, 45°, 90°, 135°, 180°, 225°, 270°, and 315 ° as shown in (Fig. 19).

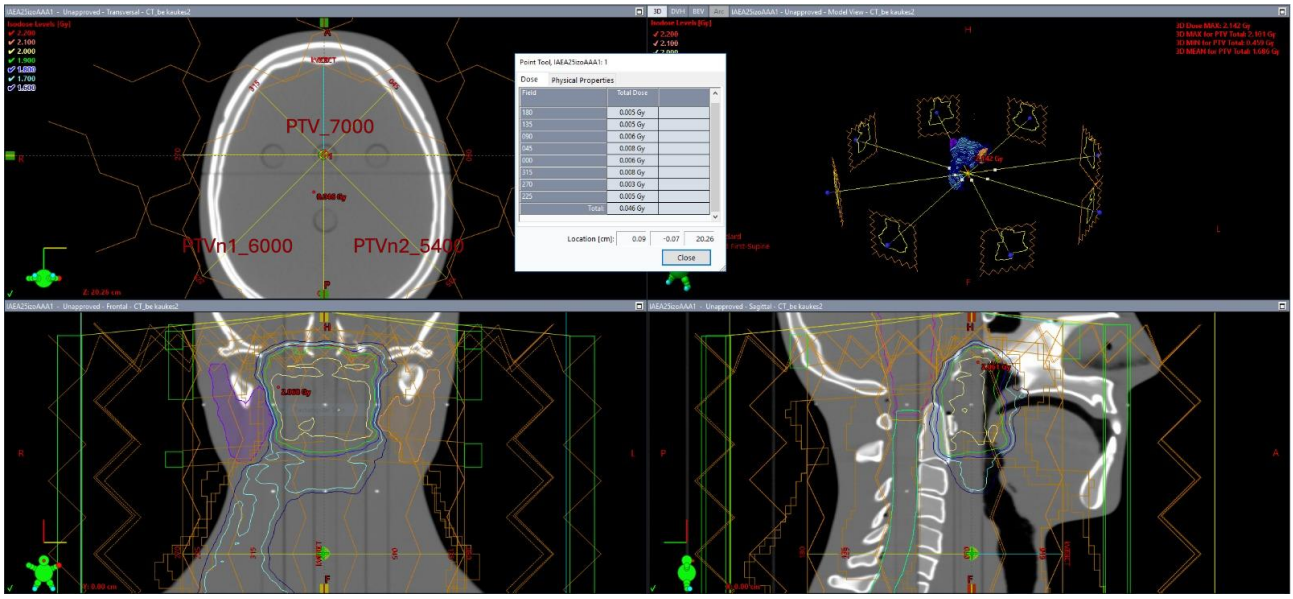

Fig. 19. IMRT out-of-field dose assessment with SHANE phantom

Out-of-field doses measurements were performed using cylindrical ionization chamber *PTW 30013* (1D dosimetry) connected to electrometer *UNIDOS T10002* using a fibre type cable. The PTW 30013 is a Farmer-type cylindrical chamber widely recognized for its high precision in absorbed dose measurements. Under standard reference conditions, it has a typical measurement uncertainty of ±1%. However, for low-dose regions such as out-of-field areas, the uncertainty may increase slightly, with reported values ranging between ±2% and ±3%, primarily due to low signal levels and scattered radiation [94]. To assess the spatial distribution of out-of-field radiation doses, measurements were conducted at 11 predefined points spaced at 2 cm intervals (ranging from 0 to 22 cm) within the SHANE anthropomorphic phantom. The region from 0 to 7 cm was designated as the out-of-field zone. The ion chamber was positioned along four anatomically relevant cylindrical channels: channel 1 aligned between the spine and trachea, channel 2 approximating the right parotid gland, channel 3 near the left parotid gland, and channel 4 located posteriorly to represent the spinal cord (Fig. 20).

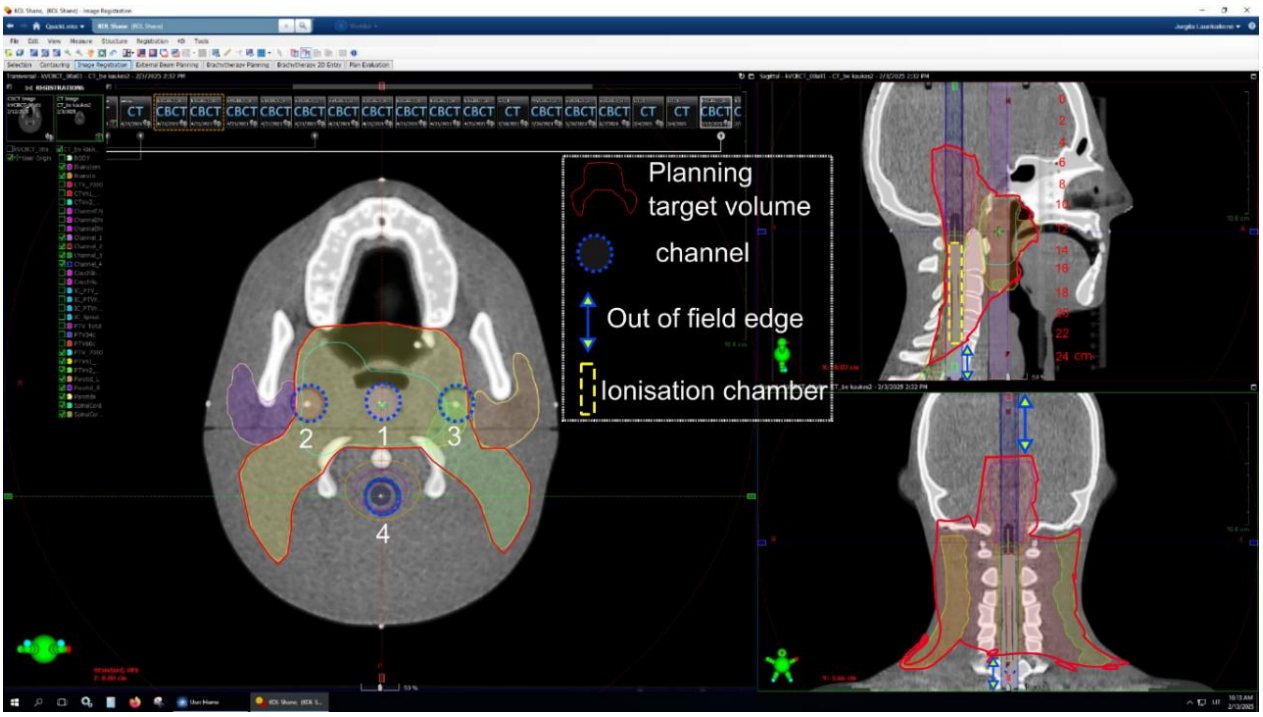

Fig. 20. Position of the channels and ionization chamber in SHANE phantom

To ensure consistent positioning of the ion chamber within the measurement cavities, phantom SHANE spacer plugs (Fig. 21) were used to fill any remaining space and maintain the position of ionisation chamber at the centre of the cavity. These measurement points were selected to characterize the dose fall-off beyond the primary treatment field and to assess the exposure to tissues located at varying distances from the target volume. The phantom was aligned to the isocentre, and the treatment plan was delivered.

Fig. 21. Spacer plugs used for the ionisation chamber positioning

During each irradiation, the ionization chamber recorded the charge produced by ionizing radiation, which was read in nanocoulombs (nC) by the electrometer. To ensure accurate absorbed dose calculation, raw readings were corrected for ambient temperature and pressure using the temperature-pressure correction coefficient *kT,P* in accordance with the IAEA TRS-398 dosimetry protocol [94]. The temperature-pressure correction factor compensates for variations in air density inside the chamber that can affect ionization. The correction is calculated using the following equation:

$$K_{T,P} = \frac{273.2 + T}{273.2 + T_0} \frac{P_0}{P} \tag{3}$$

Where *T0* and *P0* represent the standard temperature and pressure, respectively, while T and P denote the measured values of temperature and pressure.
The readings were converted to absorbed dose using the ionisation chamber calibration factor of 0.05389 Gy/nC for a 6 MV photon beam, which was traceable to a primary standards laboratory. The measurement procedure adhered to TRS-398 formalism, applying the standard equation

$$D_w = M.N_{D,W}.K_{Q,Q0} \tag{4}$$

Where *M* is the corrected electrometer reading in (nC); *ND,W* is the chamber calibration coefficient here equal to 0.05389 Gy/nC, traceable to a primary standards laboratory, *KQ,Q0* is beam quality correction factor.

These calculations provide highly accurate absorbed dose values at each point within the phantom. The accuracy of the dose depends critically on the correct application of the *kTP* correction, especially in low-dose regions typical of out-of-field exposures. Errors in temperature or pressure readings could introduce deviations in absorbed dose values, underscoring the importance of environmental monitoring during measurements.

To evaluate the accuracy of dose prediction algorithms, calculated doses from the *Eclipse* Treatment Planning System were extracted for the same positions using two algorithms: Anisotropic Analytical Algorithm (AAA) and *Acuros* XB (AC). The comparison of these calculated doses with measured values allowed for the assessment of each algorithm's performance in modelling out-of-field dose distributions.

2.5. Excess Absolute Risk Estimation

The BEIR VII committee relied heavily on radiation effects research foundation (RERF) studies on atomic bomb survivors [78]. They used two main models of excess relative risk (*ERR*) and excess absolute risk (*EAR*) [79]. BEIR VII model equation for *EAR*:

$$EAR = \beta_S Dexp(\gamma e^*)(\frac{a}{60})^n \quad (5)$$

D – dose [Sv], *e* – age at exposure [y], *e** – attained age [y], β_s – excess relative risk per sievert [EAR/Sv], γ and η being associated parameters for EAR/Sv

Table 4. Parameters in (BEIR VII model - Phase 2, table 12-2) [95]

Model parameter	Male	Female
βs	0.85	1.35
η	0.18	0.18
γ	-0.14	-0.41

2.6. EAR estimation from measured out-of-field dose

To assess the impact of treatment planning system (TPS) dose underestimation on secondary cancer risk, the Excess Absolute Risk (EAR) model was employed. This analysis focused on the brainstem, a representative organ at risk (OAR), situated 7 cm from the edge of the treatment field. Dose measurements were obtained from channel 4 of the SHANE anthropomorphic phantom. Both TPS-calculated and physically measured doses were recorded using the Anisotropic Analytical Algorithm (AAA) and *Acuros* XB (AXB) algorithms. To simulate a full course of treatment delivering 70 Gy to the primary field, doses per fraction were multiplied by 35 fractions. The EAR was adjusted using a linear dose-risk relationship, as follows:

$$Adjusted\ EAR = Baseline\ EAR \times \left(\frac{Measured\ Dose}{TPS\ Dose}\right) \quad (6)$$

This allowed quantification of EAR increase due to underestimation of out-of-field doses by TPS.

2.7. *R*-Statistical Analysis

Statistical analyses were performed using *R* statistical software (*R* Foundation for Statistical Computing, Vienna, Austria). A significance level of $p < 0.05$ was used for all statistical tests. Linear regression analysis was used to assess the relationship between patient age, gender, and the radiation dose received by specific organs. The following model was used:

$$Organ\ Dose = \beta_0 + \beta_1(Age) + \beta_2(Gender) + \epsilon \quad (7)$$

Where $\beta 0$ is the intercept; $\beta 1$ is the coefficient for age; $\beta 2$ is the coefficient for gender; ε is the error term.

The Kruskal-Wallis test was utilized to assess whether there were statistically significant differences in *EAR* across disease stages and TNM classifications. This non-parametric test was chosen due to the non-normal distribution of *EAR* data, allowing for robust comparisons among multiple independent groups. The test outputs the chi-squared statistics, degrees of freedom, and *p*-values, with a significance threshold set at $\alpha = 0.05$.

3. Results and Discussion

3.1. Incidence of Head and Neck Cancer by Age, Gender and Anatomical site

This study revealed a distinct age-related trend in head and neck cancer (HNC) incidence. The highest prevalence was observed in individuals aged 60–69 years, accounting for 54.2 % of all cases, followed by 20.3 % in the 50–59 age group and 16.9 % in those aged 70 and above. The lowest incidence was noted in patients aged 40–49, comprising only 8.47 % of the total. This distribution aligns with findings in literature, where advanced age is associated with increased cancer risk due to prolonged carcinogenic exposure and declining immune and DNA repair function [96] (Fig. 22).

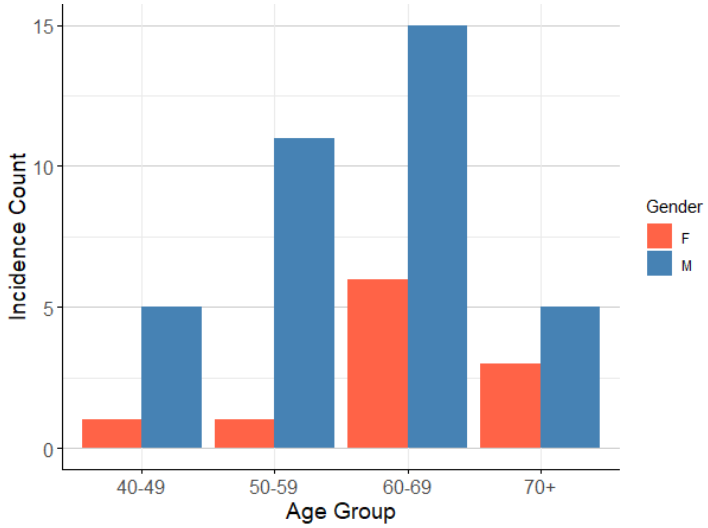

Fig. 22. Head and neck cancer by age and gender

The relatively low incidence in the 40–49 age group highlights an opportunity for early intervention. Targeted public health measures such as smoking, alcohol reduction, and early screening could significantly mitigate future HNC incidence as this population ages. Gender disparities were also pronounced in this research project. As it was shown (Fig. 22), males represented 82.2 % of cases, while females accounted for just 17.8 %. This disproportion is well-documented in epidemiological literature and may stem from behavioural, occupational, and biological factors. Higher rates of tobacco and alcohol use among men, greater exposure to industrial carcinogens, and possible differences in hormonal or genetic susceptibility all contribute to this variation [97]. Additionally, social and healthcare access disparities may further exacerbate this inequality. Therefore, these findings underscore the importance of age-and gender-specific prevention strategies in HNC management and survivorship care.

Meanwhile, variation significant of the incidence of head and neck cancers (HNC) by anatomical subsite and gender were observed. As depicted (Fig. 23) the oral cavity exhibits the highest incidence, with males accounting for 29.7 % and females for 9.32 % of cases. The oropharynx follows, with 19.5 % in males and 5.93% in females. Notably, the larynx shows a marked gender disparity, with 14.4 % of cases in males compared to 0.847 % in females. Similarly, the hypopharynx presents an incidence of 16.1 % in males versus 0.847 % in females.

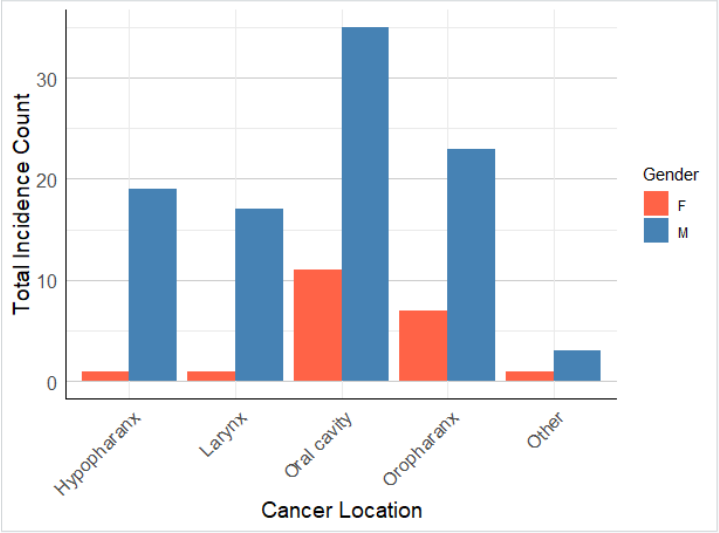

Fig. 23. Head and neck cancer incidence by anatomical sites and gender

These findings align with established epidemiological patterns. Subsites such as the oral cavity and oropharynx are more frequently exposed to environmental carcinogens like tobacco smoke and oncogenic viruses such as human papillomavirus (HPV), leading to higher incidence rates in these areas.

3.2. Influence of age and gender on organ radiation doses

The analysis of organ radiation doses in relation to age and gender provides crucial insights into how these demographic factors may influence exposure during head and neck cancer (HNC) treatment. The results of the linear regression analysis, dose of each organ was evaluated based on the contributions of age and gender as predictor variables Table 5.

Table 5. Linear regression results for organ doses

Organ	Coefficient (Intercept)	Coefficient (Age)	*p*-Value (Age)	Coefficient (Gender - M)	*p*-Value (Gender)	*R*-squared
Oesophagus	30.29129	-0.21698	0.02992	-1.22600	0.55706	0.04096
Submandibular gland (left)	40.03387	-0.00139	0.99343	3.53772	0.32253	0.00870
Submandibular gland (right)	49.60378	-0.13161	0.46189	1.53469	0.68394	0.00701
Larynx	48.22757	-0.17659	0.13458	-0.77720	0.75376	0.01945
Parotid gland (left)	24.65520	-0.13696	0.08243	2.10974	0.20329	0.04521
Parotid gland (right)	30.48843	-0.13508	0.17674	-3.93633	0.06294	0.03965
Both parotid gland	25.41695	-0.12076	0.03159	0.26599	0.82063	0.04187
Spinal cord	44.20501	-0.06973	0.26146	-0.85020	0.51552	0.01305

It was found that the regression analysis demonstrated a statistically significant inverse relationship between patient age and the radiation dose to the oesophagus (Fig. 24). Specifically, the age coefficient is -0.217 (p = 0.0299), indicating that each additional year of age is associated with an approximate 0.217 Gy reduction in oesophageal radiation dose. This trend may reflect clinical decisions to limit radiation exposure in older patients, acknowledging age-related declines in tissue repair capacity and increased susceptibility to radiation-induced toxicity.

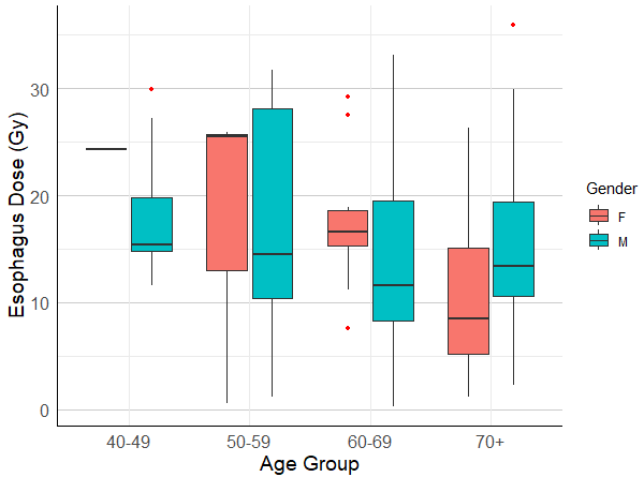

Fig. 24. Age group and gender variation in organ radiation doses for oesophagus organ

In contrast, it was found that gender does not appear to influence significantly oesophageal radiation dosage. The regression model yields a gender coefficient of -1.226 with a *p*-value of 0.557, suggesting no statistically significant difference in doses received by males compared to females. However, it is important to note that some [86], have reported gender-based differences in radiosensitivity and treatment outcomes. For example, a study [98] found that younger females exhibited higher cancer risks from radiation exposure compared to the male counterparts, emphasizing the need for further research into gender-specific responses to radiation therapy.

The presence of outliers across various age and gender groups highlights the importance of individualized treatment planning. Such variability underscores the need to consider patient-specific anatomical and tumour characteristics when determining radiation dosing, ensuring optimal therapeutic outcomes while minimizing potential adverse effects.

In comparison, for the parotid gland (Fig. 25), the age coefficient was determined as -0.1208 (p = 0.0316), which shows a strong negative link, supporting the idea that older patients may need adjusted treatment plans to ensure they are safe and effective. However, the analysis indicated that the influence of gender on radiation doses is minimal, with coefficients indicating that there is no significant difference in doses received by males compared to females for the various organs tested. In particular, the *p*-values associated with gender have been largely higher than the conventional significance threshold (α = 0.05), suggesting that treatment protocols may not adjust according to gender differences.

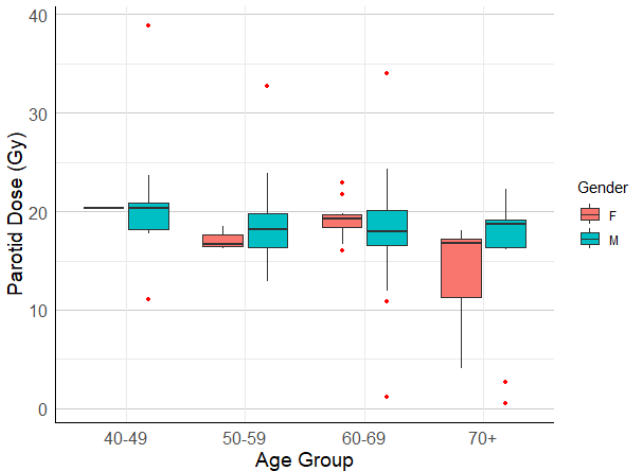

Fig. 25. Age group and gender variation in organ radiation doses for parotids organ

This aligns with research indicating that existing protocols may not fully account for potential gender-based differences in tumour biology and treatment response. Furthermore, the *R*-square values in the regressions were generally low, reflecting that these models explain a limited fraction of variance in organ doses. For example, the highest recorded *R*-squared value was 0.04522 for the parotid gland, indicating that while age and gender may play a role in dose distribution, other influencing factors, potentially including tumour type, clinical condition, or specific treatment modalities, are likely to contribute to dose variability.

3.3. Influence of tumour location and stage on excess absolute risk (EAR)

3.3.1. Excess absolute risk (EAR) by Disease Stage

Building on the analysis of demographic factors, the next step was to explore the influence of tumour location and disease stage on excess absolute risk (*EAR*). Before examining the data, it was important to clarify what the cancer stages were denoted:

- Stage I: tumours are localized and small, typically non-invasive, with no lymph node involvement.
- Stage II: tumours are larger and may have spread to nearby lymph nodes but remain localised.
- Stage III: tumours are often larger or have spread to regional lymph nodes and surrounding tissues, indicating more extensive disease.
- Stage IV: tumours have metastasized to distant parts of the body, signifying advanced disease.
- Stage X: this labelling may refer to cases with unknown primary tumours or classification when conventional staging is not applicable.

The mean *EAR*, standard deviation (*SD*), and percentage of patients for different stages of the disease, providing crucial insights into how radiation exposure risk varies with cancer progression is presented in Table 6.

Table 6. Mean Excess Absolute Risk (*EAR*) by Disease Stage

Stage	Mean *EAR*	*SD EAR*	Percentage of patients (%)
I	0.375	0.214	4.241
II	0.499	0.381	8.470
II	0.604	0.393	6.782
IV	0.789	0.513	55.931
X	0.619	0.415	24.583

As presented in Table 6, there is a progressive increase in mean *EAR* with advancing disease stage. Stage I patients exhibit a mean *EAR* of 0.375, reflecting a relatively low risk associated with localized and less aggressive tumours. As the disease progresses to Stage II and III, the mean *EAR* increases to 0.499 and 0.604, respectively, suggesting that even slight advancements in disease can result in heightened risk. The most significant increase was observed in Stage IV, with a mean *EAR* of 0.789, indicating a substantial elevation in risk. This escalation may be attributed to factors such as tumour metastasis, increased aggressiveness, and the necessity for more complex treatment protocols involving higher radiation doses to target multiple tumour sites. Stage X, often associated with unknown primary tumours or challenging classifications, presented a mean *EAR* of 0.619, underscoring the complexities in assessing risk and tailoring therapeutic interventions in such cases.

This variability indicated that while multiple patients may be at high risk because of similar treatment characteristics, some cases might have high risk due to tumour factors or individual biological

reaction to radiation. Thus, these findings emphasize the importance of individualized treatment approaches according to different stage of disease for enhancement of therapeutic effects and reduction of undesirable effects. For example, it can be seen that (Fig. 26) patients with high-grade tumours may need closer surveillance and dose refinement for optimal outcome with the least toxicity.

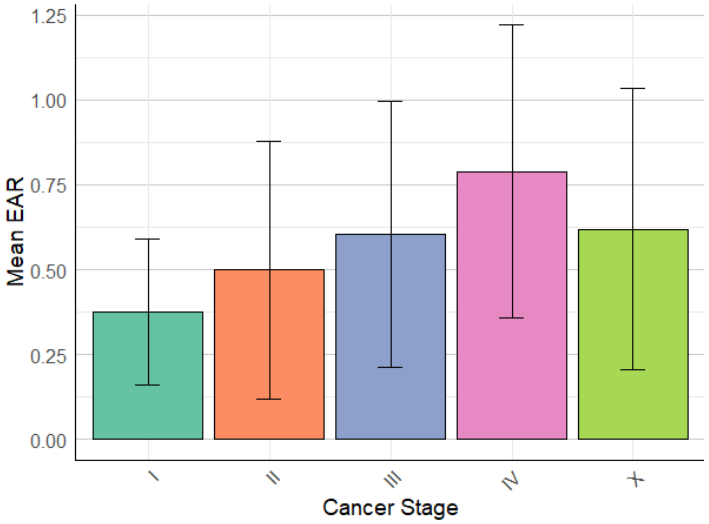

Fig. 26. Mean excess absolute risk by cancer stage

3.3.2. Excess absolute risk by TNM classification

Following exploration of the stage of the disease, we further evaluated the influence of the Tumour-Node-Metastasis (TNM) classification on Excess Absolute Risk (*EAR*). The data presented in Table 7 delineates the mean *EAR* and standard deviation for various TNM classifications, shedding light on how radiation exposure risk varies with tumour characteristics.

Table 7. Mean excess absolute risk (*EAR*) by TNM classification

TNM Classification	***Mean EAR***	***SD EAR***
T1_N0_M0	0.4341	0.3297
T1_N2_M0	0.4606	0.4742
T1_N3_M0	0.4955	0.4104
T2_N0_M0	0.5222	0.4150

Table 8. Mean excess absolute risk (*EAR*) by TNM classification (Continued)

TNM Classification	*Mean EAR*	*SD EAR*
T2_N1_M0	0.5988	0.4294
T2_N2_M0	0.6426	0.4326
T2_N3_M0	0.5542	0.3742
T3_N0_M0	0.6000	0.3571
T3_N1_M0	0.6931	0.4196
T3_N2_M0	0.6901	0.4307
T3_N3_M0	0.7375	0.5157
T3_NX_M0	0.7065	0.4418
T4_N0_M0	0.6238	0.3717
T4_N1_M0	0.8307	0.4219
T4_N2_M0	0.7148	0.4355
T4_N3_M0	0.5751	0.3883

The data revealed a clear relationship between *Mean EAR* and the TNM classification, with values generally increasing as the TNM stage becomes more advanced. As highlighted in the previous section, the emphasis on individual disease stage is echoed here, with the transition from T1 (early-stage) tumours to T4 (advanced-stage) tumours exhibiting a corresponding rise in *Mean EAR*. In particular, the highest *Mean EAR* of 0.8307 was observed in the T4_N1_M0 classification, indicating that increased tumour size and lymph node involvement correlate with elevated *EAR* values. This trend reinforces the concept that *EAR* may reflect not only the severity of the disease, but also its aggressiveness. The observed increase in *Mean EAR* alongside higher TNM classifications suggested that advanced tumours may exhibit enhanced metabolic activity and altered tumour microenvironment, both of which could be captured by *EAR* measurement.
Furthermore, as depicted in (Fig. 27), the visual representation of these relationships provided clarity on how risk escalates with increasing tumour burden and complexity.

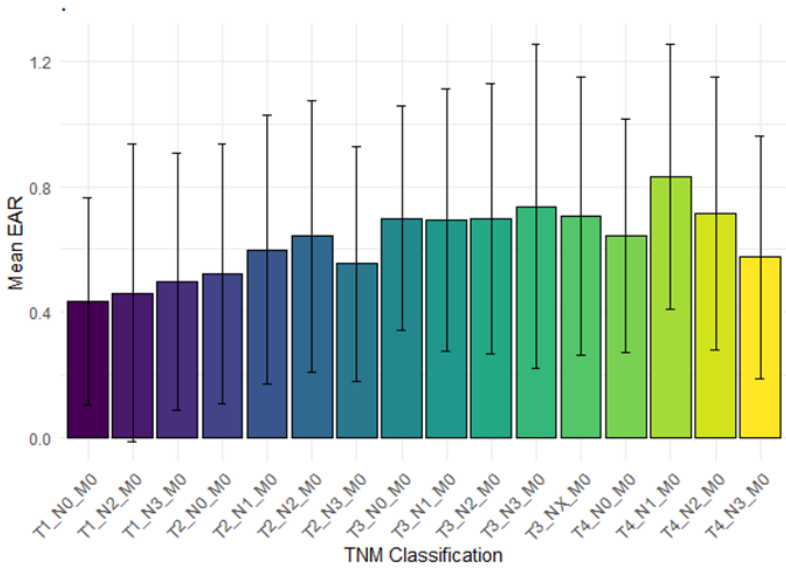

Fig. 27. Mean *EAR* by TNM classification

Understanding these underlying biological processes can significantly aid in refining prognostic assessments, as clinicians strive to develop tailored treatment strategies that optimize patient outcomes.

3.4. Out-of-field Doses Measurements

This section focuses on out-of-field dose estimation simulating head and neck cancer (HNC) case radiotherapy, building upon the previous analyses of demographic and clinical factors that influence excess absolute risk (*EAR*). Specifically, for these results to obtain was used the anthropomorphic phantom SHANE to measure irradiation doses outside the main treatment area, which is a critical step evaluating doses for the organs at risk (OARs), especially in older or more sensitive patients.

As outlined in the materials and methods section, dosimetry measurements with cylindrical ionization chamber were performed at 11 different points (in 2 cm step) along four defined channels: Channel 1, Channel 2, Channel 3, and Channel 4 as shown in Table 9 and (Fig. 28) (more detailed and visualized information of the experimental set-up is presented in Materials and methods section).

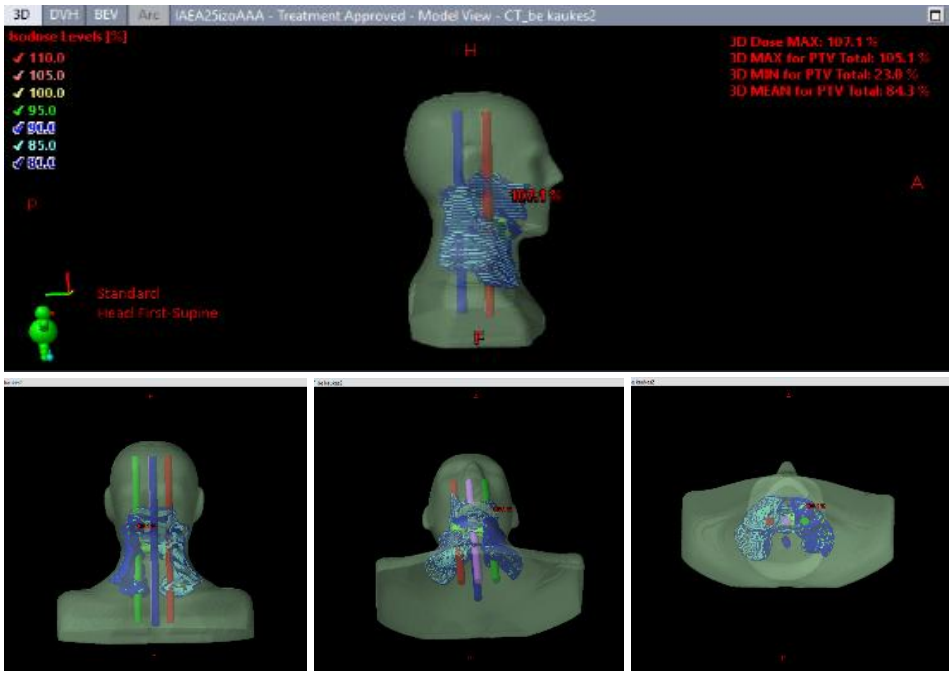

Fig. 28. Views of all the measurement channels (Channel 1 – purple; Channel 2 – red; Channel 3 – green; Channel 4 – blue) showed in different projections

Table 9. Absolute percentage error between measured and TPS calculated out-of-field doses using for the dose calculation AAA and Acuros XB algorithms throughout four anatomical channels

Position of ionization chamber in a channel, cm	Channel 1 - purple		Channel 2 - red		Channel 3 - green		Channel 4 - blue	
	Percentage error (MD vs. TPS), %							
	AAA	AC	AAA	AC	AAA	AC	AAA	AC
0	42.3	41.4	46.4	44.0	44.9	41.1	51.1 %	57.1 %
2	19.0	24.0	17.6	20.0	22.2	20.9	28.9 %	26.8 %
4	16.3	17.4	16.5	17.2	14.7	10.6	25.9 %	18.9 %
6	13.4	15.3	7.6	15.6	16.4	11.4	10.0 %	19.4 %
8	4.3	13.7	3.4	6.1	5.5	2.7	7.9 %	5.3 %
10	0.6	2.5	1.5	3.6	0.2	1.2	3.3 %	1.5 %
12	1.5	2.1	2.0	9.0	5.7	2.6	4.3 %	7.3 %
14	2.1	11.2	3.9	8.4	0.5	3.6	16.6 %	21.3 %
16	6.4	11.9	0.8	3.0	3.1	3.8	13.4 %	21.6 %
18	2.5	8.2	2.3	7.2	0.1	1.6	14.6 %	12.2 %
20	2.9	9.5	5.8	5.4	0.7	0.4	8.5 %	12.9 %
22	2.6	10.0	4.8	4.1	0.3	1.4	13.3 %	23.4 %

Out-of-field doses were measured in a distance from the edge of the irradiation field (from 0 cm up to 7 cm), as imitating head and neck cancer irradiation procedure, longitudinal target with lymph nodes zone was equal to 12 cm. It is recommended to perform additional measurements imitating larger distances (>10 cm) from the edge of irradiation field. It was registered that for the maximum up to 7 cm distances from the irradiation field edge maximum percentage differences in a Channel 4 – blue was 51.1 % (AAA) and 57.1 % (*Acuros* XB – AC) (Fig. 29). As it is reported [99] in a distance from the irradiation field edge >10 cm out-of-field doses can be underestimated up to 100 %, the same underestimation tendency was observed in comparison TPS data vs. Monte Carlo simulations.

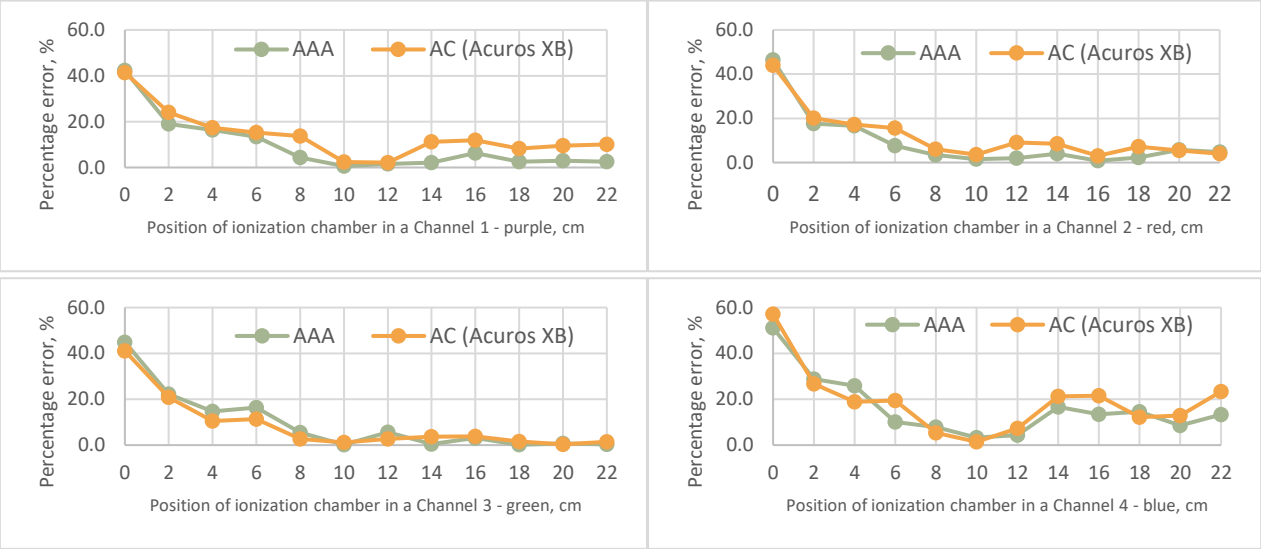

Fig. 29. Comparison of percentage errors for measured and treatment planning system (TPS) calculated out-of-field doses using AAA and Acuros XB (AC) algorithms throughout four anatomical channels

As could be expected a significant difference between calculation algorithms (AAA and *Acuros* XB) was not observed. As it is known that for such localisations like head & neck and pelvis region cancers there is no significant difference between these calculation algorithms due to the quite homogeneous densities regions. So, planning treatment of head and neck cancer cases for the dose calculation could be equally chosen AAA or *Acuros* XB algorithm.

Analysing results in all four channels (from 18 cm up to 22 cm) was noticed underestimation of the out-of-field doses, this could be influenced by the decrease of the scattered radiation or even the slightest positioning of the ionisation chamber in one or another direction [100]. The full data of the performed out-of-field doses measurements and corresponding absolute percentage errors/differences for all channels are provided in (Appendix 2).

In clinical contexts, such out-of-field doses deviations can significantly affect the risk assessment for out-of-field organs, especially for such critical organs like parotid glands and spinal cord, which are highly sensitive to radiation-induced damage. The consistent discrepancies of up to 57 % underscore the need for direct dosimetry verification during treatment planning, particularly for long-term survivors or patients at increased risk of radiation-induced late effects. Therefore, reliance on TPS calculations alone may be insufficient for accurate dose assessment in critical organs, and direct ionization chamber or other type dosimetry measurements should be integrated into routine dosimetry protocols whenever feasible.

Differences of the out-of-field doses for the simulated HNC treatment procedure using Channel 4 – blue data (as in this channel the maximum differences between measured and calculated values were determined) are summarized in Table 10.

Table 10. The EAR calculations for the brainstem (imitating the largest possible 7 cm distance from the irradiation field edge)

Parameter	**AAA**	**AXB**
TPS-calculated dose per 2 Gy fraction	0.13 Gy	0.15 Gy
Measured dose per 2 Gy fraction	0.16 Gy	0.18 Gy
TPS total dose over 35 fractions (70 Gy)	4.55 Gy	5.25 Gy
Measured total dose over 35 fractions (70 Gy)	5.60 Gy	6.40 Gy
Baseline EAR	1.00	1.00
Adjusted EAR based on measured dose	1.28	1.23
Increase in EAR (%)	23 %	22 %

These findings reveal a notable increase in Excess Absolute Risk (EAR) (23 % using the AAA algorithm and by 22 % using the *Acuros* XB (AXB) algorithm) due to the underestimation of out-of-field doses by the treatment planning system (TPS). This emphasizes the clinical significance of verifying out-of-field radiation doses through physical measurements, particularly for radiosensitive organs such as the brainstem.

Although the total accumulated dose to the brainstem in this scenario remains well below the widely accepted constraint of 54 Gy, such discrepancies could be more consequential for other organs at risk (OARs) or in different clinical contexts. Repeated underestimations across multiple treatment sessions or fields may result in cumulative doses that approach or exceed clinical tolerance limits, thereby elevating the risk of radiation-induced complications.

3.5. Recommendations for the Improved Dose Accuracy and Risk Reduction

Based on the measured out-of-field doses across four anatomical channels and the evaluation of doses calculated with TPS algorithms (*AAA* and *Acuros XB*), several key recommendations can be made to refine clinically applied dose limitation constraints and support more accurate risk estimation of secondary malignancies for HNC cases irradiation:

- The experimental data demonstrate that treatment planning systems (TPS), particularly the *Acuros* XB algorithm, consistently underestimate out-of-field doses to organs located beyond 10 cm from the irradiation field edge. For example, underestimations reached up to 47.49 % in Channel 3 (left parotid region) and 37.81 % in Channel 4 (spinal cord region), with the highest observed discrepancy being 57.1 % at 0 cm in Channel 4. These findings highlight the need to revise dose constraints for organs at risk (OARs) by including additional safety margins that reflect these systematic TPS limitations.

- Out-of-field TPS-calculated doses should be complemented with direct measurements—using ionization chambers or in vivo dosimeters particularly for radiosensitive, non-regenerative structures such as the spinal cord, parotid glands, thyroid, and gonads. This is especially important in paediatric, young adult (< 40 years), or long-term survivor populations, where the lifetime risk of secondary malignancy is a major clinical consideration. The use of anthropomorphic phantoms (e.g., SHANE) or in vivo tools ensures more accurate estimation of cumulative exposure, maintaining compliance with evidence-based dose thresholds.

- TPS reliability for out-of-field dose estimation significantly decreases at distances beyond 10 cm from the field edge. According to the measurements, percentage errors remain within 5–20 % up to 10 cm but increase dramatically (up to 23.4 %) beyond 18 cm, with trends indicating worsening accuracy with distance. Therefore, it is recommended to limit TPS-based dose calculations to within approximately 10 cm of the treatment field. For organs located further away, additional phantom-based dosimetry or Monte Carlo simulations should be employed to ensure accurate dose quantification and protect critical structures.

Conclusions

1. A significant inverse correlation was found between patient age and parotid gland dose (p = 0.0316), with older patients receiving lower doses likely reflecting efforts to reduce toxicity in this group. No notable gender-based differences were observed, suggesting current treatment plans may not consider anatomical or biological variations by gender. These results support the potential benefit of introducing age-specific dose constraints in head and neck radiotherapy to improve treatment safety and personalization.
2. The calculated Excess Absolute Risk (EAR) of secondary cancers increased progressively with tumour stage. Patients with Stage IV disease, particularly those classified as T4_N1_M0, exhibited the highest EAR values of 0.789 and 0.8307, respectively. This underscores a strong association between disease severity and radiation-induced cancer risk. These results advocate for stage-adapted radiotherapy approaches that incorporate tumour burden and patient-specific clinical factors into risk assessment, with the aim of minimizing long-term complications and optimizing treatment outcomes.
3. Both AAA as well as *Acuros* XB algorithms available in the Eclipse TPS underestimated out-of-field doses. It was found that the largest difference (57.1 % between TPS calculated and measured) was registered in 7 cm distance from the field edge (Channel 4 – blue). For the further investigation it is warranted to evaluate out-of-field dose discrepancies and associated risks at greater distances from the treatment field, where TPS predictions may be even less reliable.
4. It was determined that EAR increased by 23% (AAA) and 22% (*Acuro*s XB) in the largest possible measured distance (7 cm) based on measured versus TPS-calculated doses over 35 fractions (2 Gy/ fr.). This underlines the clinical impact of TPS underestimation in out-of-field regions. Incorporating direct dose verification and EAR-based evaluation into treatment planning process could improve accuracy of the dose constraints and reduce long-term risks in radiotherapy.

Acknowledgement

I would like to express my deepest gratitude to my supervisor, Assoc. Prof. Dr. Jurgita Laurikaitienė, for her thoughtful guidance, continuous encouragement, and unwavering support throughout this work. Her knowledge and clarity helped shape this study in meaningful ways. I am sincerely thankful to Assoc. Prof. Dr. Kristina Šutienė for her valuable assistance, particularly in the statistical analysis, her readiness to help and her expertise were a great asset. To my family, thank you for your patience, understanding, and constant encouragement. A special thanks goes to my husband, whose quiet strength, love, and support have been my anchor throughout this journey. And to my daughter, who has been a daily source of joy and inspiration even when she didn't understand why I had to spend so many hours working, her smiles reminded me what all this was for.

References

1. MARUR, Shanthi and FORASTIERE, Arlene A. *Head and Neck Squamous Cell Carcinoma: Update on Epidemiology, Diagnosis, and Treatment*. 1 March 2016. Elsevier Ltd.
2. ALTERIO, Daniela, MARVASO, Giulia, FERRARI, Annamaria, VOLPE, Stefania, ORECCHIA, Roberto and JERECZEK-FOSSA, Barbara Alicja. *Modern radiotherapy for head and neck cancer*. 1 June 2019. W.B. Saunders.
3. SHINE, N. S., PARAMU, Raghukumar, GOPINATH, M., JAON BOS, R. C. and JAYADEVAN, P. M. Out-of-field dose calculation by a commercial treatment planning system and comparison by monte carlo simulation for varian TrueBeam®. *Journal of Medical Physics*. 1 July 2019. Vol. 44, no. 3, p. 156–175. DOI 10.4103/jmp.JMP_82_18.
4. PAZZAGLIA, S., EIDEMÜLLER, M., LUMNICZKY, K., MANCUSO, M., RAMADAN, R., STOLARCZYK, L. and MOERTL, S. Out-of-field effects: lessons learned from partial body exposure. *Radiation and Environmental Biophysics*. 1 November 2022. Vol. 61, no. 4, p. 485–504. DOI 10.1007/s00411-022-00988-0.
5. DRACHAM, C. B., Sharonjeet, K., & Rashmi, R. Radiation induced secondary cancers: a review article. *Radiation Oncology Journal*. 2018. Vol. 36, no. 2, p. 85.
6. MODY, Mayur D., ROCCO, James W., YOM, Sue S., HADDAD, Robert I. and SABA, Nabil F. *Head and neck cancer*. 18 December 2021. Elsevier B.V.
7. REID, Paul, WILSON, Puthenparampil, LI, Yanrui, MARCU, Loredana G., STAUDACHER, Alexander H., BROWN, Michael P. and BEZAK, Eva. Experimental investigation of radiobiology in head and neck cancer cell lines as a function of HPV status, by MTT assay. *Scientific Reports*. 1 December 2018. Vol. 8, no. 1. DOI 10.1038/s41598-018-26134-9.
8. ROMAN, Benjamin R. and ARAGONES, Abraham. *Epidemiology and incidence of HPV-related cancers of the head and neck*. 1 November 2021. John Wiley and Sons Inc.
9. SABATINI, Maria Elisa and CHIOCCA, Susanna. *Human papillomavirus as a driver of head and neck cancers*. 4 February 2020. Springer Nature.
10. GALLI, Federica, RUSPI, Laura, MARZORATI, Alessandro, LAVAZZA, Matteo, DI ROCCO, Giuseppe, BONI, Luigi, DIONIGI, Gianlorenzo and RAUSEI, Stefano. *N staging system: Tumor-node-metastasis and future perspectives*. 2017. AME Publishing Company.
11. YUAN, Ping, CAO, Jin Lin, RUSTAM, Azmat, ZHANG, Chong, YUAN, Xiao Shuai, BAO, Fei Chao, LV, Wang and HU, Jian. Time-To-Progression of NSCLC from Early to Advanced Stages: An Analysis of data from SEER Registry and a Single Institute. *Scientific Reports*. 27 June 2016. Vol. 6. DOI 10.1038/srep28477.
12. AMIN, Mahul B., GREENE, Frederick L., EDGE, Stephen B., COMPTON, Carolyn C., GERSHENWALD, Jeffrey E., BROOKLAND, Robert K., MEYER, Laura, GRESS, Donna M., BYRD, David R. and WINCHESTER, David P. The Eighth Edition AJCC Cancer Staging Manual: Continuing to build a bridge from a population-based to a more "personalized" approach to cancer staging . *CA: A Cancer Journal for Clinicians*. March 2017. Vol. 67, no. 2, p. 93–99. DOI 10.3322/caac.21388.
13. INUYAMA, Y., FUJII, M., TANAKA, J., TAKAOKA, T., HOSODA, H. and KOHNO, N. Multidisciplinary treatment of head and neck cancer. *Gan no rinsho. Japan journal of cancer clinics*. July 1985. Vol. 31, no. 9 Suppl, p. 1051–1056. DOI 10.1055/s-0030-1263075.
14. BASKAR, Rajamanickam, LEE, Kuo Ann, YEO, Richard and YEOH, Kheng Wei. *Cancer and radiation therapy: Current advances and future directions*. 27 February 2012.

15. HANSEN, Christian Rønn, BERTELSEN, Anders, HAZELL, Irene, ZUKAUSKAITE, Ruta, GYLDENKERNE, Niels, JOHANSEN, Jørgen, ERIKSEN, Jesper G. and BRINK, Carsten. Automatic treatment planning improves the clinical quality of head and neck cancer treatment plans. *Clinical and Translational Radiation Oncology*. 1 December 2016. Vol. 1, p. 2–8. DOI 10.1016/j.ctro.2016.08.001.
16. MATSUMOTO, TADASHI, TOYA, RYO, SHIMOHIGASHI, YOSHINOBU, WATAKABE, TAKAHIRO, MATSUYAMA, TOMOHIKO, SAITO, TETSUO, FUKUGAWA, YOSHIYUKI, KAI, YUDAI and OYA, NATSUO. Plan quality comparisons between 3D-CRT, IMRT, and VMAT Based on 4D-CT for gastric MALT lymphoma. *Anticancer Research*. 1 August 2021. Vol. 41, no. 8, p. 3941–3947. DOI 10.21873/anticanres.15190.
17. MOHAMED YOOSUF, Ahamed Badusha, ALSHEHRI, Salem, ABDUL AZIZ, Mohd Zahri, MANSOR, Syahir, APPALANAIDO, Gokula Kumar and ALQATHAMI, Mamdouh. Effectiveness of Robotic Stereotactic Radiotherapy in Patients Undergoing Re-irradiation: A Review. *Cureus*. 15 August 2023. DOI 10.7759/cureus.43500.
18. BYDDER, Sean. SBRT revolution in lung radiotherapy. [online]. 3 July 2018. [Accessed 7 May 2025]. Available from: https://mforum.com.au/sbrt-revolution-in-lung-radiotherapy/
19. LEE, Percy, LOO, Billy W., BISWAS, Tithi, DING, George X., EL NAQA, Issam M., JACKSON, Andrew, KONG, Feng Ming, LACOUTURE, Tamara, MIFTEN, Moyed, SOLBERG, Timothy, TOME, Wolfgang A., TAI, An, YORKE, Ellen and LI, X. Allen. Local Control After Stereotactic Body Radiation Therapy for Stage I Non-Small Cell Lung Cancer. *International Journal of Radiation Oncology Biology Physics*. 1 May 2021. Vol. 110, no. 1, p. 160–171. DOI 10.1016/j.ijrobp.2019.03.045.
20. LAVROVA, Elizaveta, GARRETT, Matthew D., WANG, Yi Fang, CHIN, Christine, ELLISTON, Carl, SAVACOOL, Michelle, PRICE, Michael, KACHNIC, Lisa A. and HOROWITZ, David P. *Adaptive Radiation Therapy: A Review of CT-based Techniques*. 1 July 2023. Radiological Society of North America Inc.
21. DONA LEMUS, Olga Maria, CAO, Minsong, CAI, Bin, CUMMINGS, Michael and ZHENG, Dandan. *Adaptive Radiotherapy: Next-Generation Radiotherapy*. 1 March 2024. Multidisciplinary Digital Publishing Institute (MDPI).
22. N, Kiran Kumar, MERWADE, Seema, PRABAKARAN, Pavithra, C H, Laxmi Priya, B S, Annapoorna and C N, Guruprasad. *Magnetic resonance imaging versus cone beam computed tomography in diagnosis of periapical pathosis – A systematic review*. 1 December 2021. Elsevier B.V.
23. DIWANJI, Tejan P., MOHINDRA, Pranshu, VYFHUIS, Melissa, SNIDER, James W., KALAVAGUNTA, Chaitanya, MOSSAHEBI, Sina, YU, Jen, FEIGENBERG, Steven and BADIYAN, Shahed N. *Advances in radiotherapy techniques and delivery for non-small cell lung cancer: Benefits of intensity-modulated radiation therapy, proton therapy, and stereotactic body radiation therapy*. 1 April 2017. AME Publishing Company.
24. GUPTA, Tejpal, AGARWAL, Jaiprakash, JAIN, Sandeep, PHURAILATPAM, Reena, KANNAN, Sadhana, GHOSH-LASKAR, Sarbani, MURTHY, Vedang, BUDRUKKAR, Ashwini, DINSHAW, Ketayun, PRABHASH, Kumar, CHATURVEDI, Pankaj and D'CRUZ, Anil. Three-dimensional conformal radiotherapy (3D-CRT) versus intensity modulated radiation therapy (IMRT) in squamous cell carcinoma of the head and neck: A randomized controlled trial. *Radiotherapy and Oncology*. September 2012. Vol. 104, no. 3, p. 343–348. DOI 10.1016/j.radonc.2012.07.001.

25. ANTONY, Febin, K., Mathew Varghese, C., Jomon Raphael, G., Paul Gopu and SIVAKUMAR, S. Dosimetric comparison of organs at risk with three-dimensional conformal radiation, intensity-modulated radiation and volumetric-modulated arc therapy in cervical cancer: a cross sectional study. *International Journal of Advances in Medicine*. 23 March 2021. Vol. 8, no. 4, p. 586. DOI 10.18203/2349-3933.ijam20210978.
26. CHO, Byungchul. *Intensity-modulated radiation therapy: A review with a physics perspective*. 1 March 2018. Department of Radiation Oncology.
27. WEBB, S. *The physical basis of IMRT and inverse planning*. October 2003.
28. KAM, Michael K.M., LEUNG, Sing Fai, ZEE, Benny, CHAU, Ricky M.C., SUEN, Joyce J.S., MO, Frankie, LAI, Maria, HO, Rosalie, CHEUNG, Kin Yin, YU, Brian K.H., CHIU, Samuel K.W., CHOI, Peter H.K., TEO, Peter M.L., KWAN, Wing Hong and CHAN, Anthony T.C. Prospective randomized study of intensity-modulated radiotherapy on salivary gland function in early-stage nasopharyngeal carcinoma patients. *Journal of Clinical Oncology*. 1 November 2007. Vol. 25, no. 31, p. 4873–4879. DOI 10.1200/JCO.2007.11.5501.
29. SCHLICHTING, Jennifer A., PAGEDAR, Nitin A., CHIORESO, Catherine, LYNCH, Charles F. and CHARLTON, Mary E. Treatment trends in head and neck cancer: Surveillance, Epidemiology, and End Results (SEER) Patterns of Care analysis. *Cancer Causes and Control*. 1 July 2019. Vol. 30, no. 7, p. 721–732. DOI 10.1007/s10552-019-01185-z.
30. GRÉGOIRE, Vincent, LANGENDIJK, Johannes A. and NUYTS, Sandra. *Advances in radiotherapy for head and neck cancer*. 10 October 2015. American Society of Clinical Oncology.
31. DAS MAJUMDAR, Saroj Kumar, AMRITT, Adhar, DHAR, Sovan Sarang, BARIK, Sandip, BEURA, Sasanka S, MISHRA, Tushar, MUDULY, Dillip K, DASH, Ashish and PARIDA, Dillip Kumar. A Dosimetric Study Comparing 3D-CRT vs. IMRT vs. VMAT in Left-Sided Breast Cancer Patients After Mastectomy at a Tertiary Care Centre in Eastern India. *Cureus*. 28 March 2022. DOI 10.7759/cureus.23568.
32. HUNTE, Sherisse Ornella, CLARK, Catharine H., ZYUZIKOV, Nikolay and NISBET, Andrew. *Volumetric modulated arc therapy (VMAT): a review of clinical outcomes—what is the clinical evidence for the most effective implementation?* 2022. British Institute of Radiology.
33. YEH, Chi-Yuan, LAI, Peng-An, LIU, Fang-Hui and HE, Chin-Chiao. Fractionated Volumetric Modulated Arc Therapy (FVMAT) for Oligometastatic Brain Tumor. *Onco*. 2 February 2023. Vol. 3, no. 1, p. 43–52. DOI 10.3390/onco3010004.
34. PLAZA, Dominika, SROKA, Łukasz, ORZECHOWSKA, Klaudia and ŚLOSAREK, Krzysztof. commerciallyComparison of the dose distribution of the VMAT radiotherapy technique depending on the beam used: FFF-X10MV and FFF-X15MV. *Reports of Practical Oncology and Radiotherapy*. 2023. Vol. 28, no. 5, p. 654–660. DOI 10.5603/rpor.97508.
35. KAZANTSEV, Pavel, LECHNER, Wolfgang, GERSHKEVITSH, Eduard, CLARK, Catharine H., VENENCIA, Daniel, VAN DYK, Jacob, WESOLOWSKA, Paulina, HERNANDEZ, Victor, JORNET, Nuria, TOMSEJ, Milan, BOKULIC, Tomislav and IZEWSKA, Joanna. IAEA methodology for on-site end-to-end IMRT/VMAT audits: an international pilot study. *Acta Oncologica*. 1 February 2020. Vol. 59, no. 2, p. 141–148. DOI 10.1080/0284186X.2019.1685128.
36. KNAPP, Penelope, EVA, Belinda, RESEIGH, Gemma, GIBBS, Adrian, SIM, Lucy, DALY, Tiffany, COX, Judith and BERNARD, Anne. The role of volumetric modulated arc therapy (VMAT) in gynaecological radiation therapy: A dosimetric comparison of intensity modulated radiation therapy versus VMAT. *Journal of Medical Radiation Sciences*. 1 March 2019. Vol. 66, no. 1, p. 44–53. DOI 10.1002/jmrs.311.

37. CHEN, Desiree, CAI, Shao Bin, SOON, Yu Yang, CHEO, Timothy, VELLAYAPPAN, Balamurugan, TAN, Chek Wee and HO, Francis. *Dosimetric comparison between Intensity Modulated Radiation Therapy (IMRT) vs dual arc Volumetric Arc Therapy (VMAT) for nasopharyngeal cancer (NPC): Systematic review and meta-analysis*. 1 March 2023. Elsevier Inc.
38. HOWELL, Rebecca M., SCARBORO, Sarah B., KRY, S. F. and YALDO, Derek Z. Accuracy of out-of-field dose calculations by a commercial treatment planning system. *Physics in Medicine and Biology*. 7 December 2010. Vol. 55, no. 23, p. 6999–7008. DOI 10.1088/0031-9155/55/23/S03.
39. BERRINGTON DE GONZALEZ, Amy, GILBERT, Ethel, CURTIS, Rochelle, INSKIP, Peter, KLEINERMAN, Ruth, MORTON, Lindsay, RAJARAMAN, Preetha and LITTLE, Mark P. *Second solid cancers after radiation therapy: A systematic review of the epidemiologic studies of the radiation dose-response relationship*. 1 June 2013.
40. GARRETT, Lachlan, HARDCASTLE, Nicholas, YEO, Adam, LONSKI, Peta, FRANICH, Rick and KRON, Tomas. Out-of-field dose in stereotactic radiotherapy for paediatric patients. *Physics and Imaging in Radiation Oncology*. 1 July 2021. Vol. 19, p. 1–5. DOI 10.1016/j.phro.2021.05.006.
41. SÁNCHEZ-NIETO, B., MEDINA-ASCANIO, K. N., RODRÍGUEZ-MONGUA, J. L., DOERNER, E. and ESPINOZA, I. Study of out-of-field dose in photon radiotherapy: A commercial treatment planning system versus measurements and Monte Carlo simulations. *Medical Physics*. 1 September 2020. Vol. 47, no. 9, p. 4616–4625. DOI 10.1002/mp.14356.
42. RAHBAR YAZDI, Shiva, ZARE, Mohammad Hosein and BROOMAND, Mohammad Ali. Out-of-Field Dose Measurement by TLD Dosimetry and Estimation of Radiation-Induced Secondary Cancer Risk of Thyroid and Breast from Head Radiotherapy. *Journal of Biomedical Physics and Engineering*. 1 September 2023. Vol. 13, no. 5, p. 403–410. DOI 10.31661/jbpe.v0i0.2302-1595.
43. GAGNÉ, Isabelle Marie and ZAVGORODNI, Sergei. Evaluation of the analytical anisotropic algorithm in an extreme water-lung interface phantom using Monte Carlo dose calculations. *Journal of Applied Clinical Medical Physics*. 2007. Vol. 8, no. 1, p. 33–46. DOI 10.1120/jacmp.v8i1.2324.
44. OJALA, Jarkko. The accuracy of the Acuros XB algorithm in external beam radiotherapy – a comprehensive review. *International Journal of Cancer Therapy and Oncology*. 24 October 2014. Vol. 2, no. 4, p. 020417. DOI 10.14319/ijcto.0204.17.
45. HOWELL, Rebecca M., SCARBORO, Sarah B., TADDEI, Phillip J., KRISHNAN, Sunil, KRY, Stephen F. and NEWHAUSER, Wayne D. Methodology for determining doses to in-field, out-of-field and partially in-field organs for late effects studies in photon radiotherapy. *Physics in Medicine and Biology*. 7 December 2010. Vol. 55, no. 23, p. 7009–7023. DOI 10.1088/0031-9155/55/23/S04.
46. HALL, Eric J. and WUU, Cheng Shie. Radiation-induced second cancers: The impact of 3D-CRT and IMRT. *International Journal of Radiation Oncology Biology Physics*. 1 May 2003. Vol. 56, no. 1, p. 83–88. DOI 10.1016/S0360-3016(03)00073-7.
47. MATUSZAK, Natalia, KRUSZYNA-MOCHALSKA, Marta, SKROBALA, Agnieszka, RYCZKOWSKI, Adam, ROMANSKI, Piotr, PIOTROWSKI, Igor, KULCENTY, Katarzyna, SUCHORSKA, Wiktoria Maria and MALICKI, Julian. Nontarget and Out-of-Field Doses from Electron Beam Radiotherapy. *Life*. 1 June 2022. Vol. 12, no. 6. DOI 10.3390/life12060858.
48. COLNOT, Julie, ZEFKILI, Sofia, GSCHWIND, Régine and HUET, Christelle. Out-of-field doses from radiotherapy using photon beams: A comparative study for a pediatric renal treatment. *Journal of Applied Clinical Medical Physics*. 1 March 2021. Vol. 22, no. 3, p. 94–106. DOI 10.1002/acm2.13182.

49. KRY, Stephen F., BEDNARZ, Bryan, HOWELL, Rebecca M., DAUER, Larry, FOLLOWILL, David, KLEIN, Eric, PAGANETTI, Harald, WANG, Brian, WUU, Cheng Shie and GEORGE XU, X. AAPM TG 158: Measurement and calculation of doses outside the treated volume from external-beam radiation therapy. *Medical Physics*. 1 October 2017. Vol. 44, no. 10, p. e391–e429. DOI 10.1002/mp.12462.
50. MILLE, Matthew M., JUNG, Jae Won, LEE, Choonik, KUZMIN, Gleb A. and LEE, Choonsik. Comparison of normal tissue dose calculation methods for epidemiological studies of radiotherapy patients. *Journal of Radiological Protection*. 1 June 2018. Vol. 38, no. 2, p. 775–792. DOI 10.1088/1361-6498/aabd4f.
51. RANA, Suresh and ROGERS, Kevin. Dosimetric evaluation of Acuros XB dose calculation algorithm with measurements in predicting doses beyond different air gap thickness for smaller and larger field sizes. *Journal of Medical Physics*. January 2013. Vol. 38, no. 1, p. 9–14. DOI 10.4103/0971-6203.106600.
52. WANG, Lilie and DING, George X. Estimating the uncertainty of calculated out-of-field organ dose from a commercial treatment planning system. *Journal of Applied Clinical Medical Physics*. 1 July 2018. Vol. 19, no. 4, p. 319–324. DOI 10.1002/acm2.12367.
53. KRY, Stephen F., ALVAREZ, Paola, CYGLER, Joanna E., DEWERD, Larry A., HOWELL, Rebecca M., MEEKS, Sanford, O'DANIEL, Jennifer, REFT, Chester, SAWAKUCHI, Gabriel, YUKIHARA, Eduardo G. and MIHAILIDIS, Dimitris. AAPM TG 191: Clinical use of luminescent dosimeters: TLDs and OSLDs. *Medical Physics*. 1 February 2020. Vol. 47, no. 2, p. e19–e51. DOI 10.1002/mp.13839.
54. BOZYDAR KNYZIAK, Adrian and RZODKIEWICZ, Witold. Measurement methods of ionization current and electric charges in radiation dosimetry. *Nuclear Instruments and Methods in Physics Research, Section A: Accelerators, Spectrometers, Detectors and Associated Equipment*. 21 June 2016. Vol. 822, p. 1–8. DOI 10.1016/j.nima.2016.03.070.
55. CHOW, James C. L. and RUDA, Harry E. In Vivo Dosimetry in Radiotherapy: Techniques, Applications, and Future Directions. *Encyclopedia* [online]. 20 March 2025. Vol. 5, no. 1, p. 40. DOI 10.3390/encyclopedia5010040. Available from: https://www.mdpi.com/2673-8392/5/1/40
56. WALTER, Autumn E., HANSEN, Jon B. and DEWERD, Larry A. Evaluation of ionization chamber stability checks using various sources. *Physica Medica*. 1 December 2020. Vol. 80, p. 327–334. DOI 10.1016/j.ejmp.2020.11.010.
57. NIROOMAND-RAD, Azam, CHIU-TSAO, Sou Tung, GRAMS, Michael P., LEWIS, David F., SOARES, Christopher G., VAN BATTUM, Leo J., DAS, Indra J., TRICHTER, Samuel, KISSICK, Michael W., MASSILLON-JL, Guerda, ALVAREZ, Paola E. and CHAN, Maria F. Report of AAPM Task Group 235 Radiochromic Film Dosimetry: An Update to TG-55. *Medical Physics*. 1 December 2020. Vol. 47, no. 12, p. 5986–6025. DOI 10.1002/mp.14497.
58. LOW, Daniel A., MORAN, Jean M., DEMPSEY, James F., DONG, Lei and OLDHAM, Mark. Dosimetry tools and techniques for IMRT. *Medical Physics*. 2011. Vol. 38, no. 3, p. 1313–1338. DOI 10.1118/1.3514120.
59. ABDELAAL, Ahmed M., ATTALLA, Ehab M. and ELSHEMEY, Wael M. Estimation of Out-of-Field Dose Variation using Markus Ionization Chamber Detector. *SciMedicine Journal*. 1 March 2020. Vol. 2, no. 1, p. 8–15. DOI 10.28991/scimedj-2020-0201-2.
60. KRY, Stephen F., SALEHPOUR, Mohammad, FOLLOWILL, David S., STOVALL, Marilyn, KUBAN, Deborah A., WHITE, R. Allen and ROSEN, Isaac I. Out-of-field photon and neutron dose equivalents from step-and-shoot intensity-modulated radiation therapy. *International Journal of*

Radiation Oncology Biology Physics. 15 July 2005. Vol. 62, no. 4, p. 1204–1216. DOI 10.1016/j.ijrobp.2004.12.091.
61. LE GUILLOU, Mael, GRUEL, Adrien, DESTOUCHES, Christophe and BLAISE, Patrick. State of the art on nuclear heating measurement methods and expected improvements in zero power research reactors. *EPJ Nuclear Sciences & Technologies*. 2017. Vol. 3, p. 11. DOI 10.1051/epjn/2017002.
62. KINHIKAR, Rajesh, GAMRE, Poonam, TAMBE, Chandrashekhar, KADAM, Sudarshan, BIJU, George, SURYAPRAKASH, MAGAI, C. S., DHOTE, Dipak, SHRIVASTAVA, Shyam and DESHPANDE, Deepak. Peripheral dose measurements with diode and thermoluminescence dosimeters for intensity modulated radiotherapy delivered with conventional and un-conventional linear accelerator. *Journal of Medical Physics*. January 2013. Vol. 38, no. 1, p. 4–8. DOI 10.4103/0971-6203.106599.
63. ROJAS-LÓPEZ, J. A., AGÜERO, H., MANCUZO, A. and BINIA, S. Out-of-field dosimetry in IMRT with OSL. In : *AIP Conference Proceedings*. American Institute of Physics Inc., 30 April 2021. ISBN 9780735440944.
64. ZHANG, Yan, YAN, Shaojie, CUI, Zhen, WANG, Yungang, LI, Zhenjiang, YIN, Yong, LI, Baosheng, QUAN, Hong and ZHU, Jian. Out-of-field dose assessment for a 1.5 T MR-Linac with optically stimulated luminescence dosimeters. *Medical Physics*. 1 July 2021. Vol. 48, no. 7, p. 4027–4037. DOI 10.1002/mp.14839.
65. CASOLARO, Pierluigi, CAMPAJOLA, Luigi, BREGLIO, Giovanni, BUONTEMPO, Salvatore, CONSALES, Marco, CUSANO, Andrea, CUTOLO, Antonello, DI CAPUA, Francesco, FIENGA, Francesco and VAIANO, Patrizio. Real-time dosimetry with radiochromic films. *Scientific Reports*. 1 December 2019. Vol. 9, no. 1. DOI 10.1038/s41598-019-41705-0.
66. PIOTROWSKI, Igor, KULCENTY, Katarzyna, SUCHORSKA, Wiktoria, RUCINSKI, Marcin, JOPEK, Karol, KRUSZYNA-MOCHALSKA, Marta, SKROBALA, Agnieszka, ROMANSKI, Piotr, RYCZKOWSKI, Adam, BOROWICZ, Dorota, MATUSZAK, Natalia and MALICKI, Julian. Cellular Damage in the Target and Out-Of-Field Peripheral Organs during VMAT SBRT Prostate Radiotherapy: An In Vitro Phantom-Based Study. *Cancers*. 1 June 2022. Vol. 14, no. 11. DOI 10.3390/cancers14112712.
67. LEE, Nancy, PURI, Dev R., BLANCO, Angel I. and CHAO, K. S.Clifford. *Intensity-modulated radiation therapy in head and neck cancers: An update*. April 2007.
68. POW, Edmond H.N., KWONG, Dora L.W., MCMILLAN, Anne S., WONG, May C.M., SHAM, Jonathan S.T., LEUNG, Lucullus H.T. and LEUNG, W. Keung. Xerostomia and quality of life after intensity-modulated radiotherapy vs. conventional radiotherapy for early-stage nasopharyngeal carcinoma: Initial report on a randomized controlled clinical trial. *International Journal of Radiation Oncology Biology Physics*. 15 November 2006. Vol. 66, no. 4, p. 981–991. DOI 10.1016/j.ijrobp.2006.06.013.
69. TANG, Hao, CHEN, Xuming, LIU, Yang, LU, Zhipeng, YOU, Junhua, YANG, Mingzhou, YAO, Shengyu, ZHAO, Guoqi, XU, Yi, CHEN, Tingfeng, LIU, Yong and XIE, Xiaohui. Clinically applicable deep learning framework for organs at risk delineation in CT images. *Nature Machine Intelligence*. 30 September 2019. Vol. 1, no. 10, p. 480–491. DOI 10.1038/s42256-019-0099-z.
70. EISBRUCH, Avraham, FOOTE, Robert L, O'SULLIVAN, Brian, BEITLER, Jonathan J and VIKRAM, Bhadrasain. *Intensity-Modulated Radiation Therapy for Head and Neck Cancer: Em lhasis on the Selection and Delineation the Targets*. 2002.

71. MAYO, Charles, YORKE, Ellen and MERCHANT, Thomas E. Radiation Associated Brainstem Injury. *International Journal of Radiation Oncology Biology Physics*. 1 March 2010. Vol. 76, no. 3 SUPPL. DOI 10.1016/j.ijrobp.2009.08.078.
72. NG, Sweet Ping, POLLARD, Courtney, KAMAL, Mona, AYOUB, Zeina, GARDEN, Adam S., BAHIG, Houda, GUNN, G. Brandon, FRANK, Steven J., SKINNER, Heath D., PHAN, Jack, BERENDS, Joel, MORRISON, William H., JOHNSON, Jason M., FERRAROTTO, Renata, STURGIS, Erich M., MOHAMED, Abdallah S.R., LAI, Stephen Y., FULLER, Clifton D. and ROSENTHAL, David I. Risk of second primary malignancies in head and neck cancer patients treated with definitive radiotherapy. *npj Precision Oncology*. 1 December 2019. Vol. 3, no. 1. DOI 10.1038/s41698-019-0097-y.
73. FERLAY, J., Soerjomataram, I., Dikshit, R., Eser, S., Mathers, C., Rebelo, M., ... & Bray, F. Cancer incidence and mortality worldwide: sources, methods and major patterns in GLOBOCAN 2012. *International journal of cancer*. 2015. Vol. 136, no. 5, p. E359–E386.
74. KUHLIN, Beatrice, KRAMER, Benedikt, NEFAS, Vytis, ROTTER, Nicole and ADERHOLD, Christoph. Indicators for secondary carcinoma in head and neck cancer patients following curative therapy: A retrospective clinical study. *Molecular and Clinical Oncology*. 2020. Vol. 12, no. 5, p. 403–410. DOI 10.3892/mco.2020.2004.
75. BOAKYE, Eric Adjei, BUCHANAN, Paula, HINYARD, Leslie, OSAZUWA-PETERS, Nosayaba, SCHOOTMAN, Mario and PICCIRILLO, Jay F. Incidence and risk of second primary malignant neoplasm after a first head and neck squamous cell carcinoma. *JAMA Otolaryngology - Head and Neck Surgery*. 1 August 2018. Vol. 144, no. 8, p. 727–737. DOI 10.1001/jamaoto.2018.0993.
76. HADA, M., & Georgakilas, A. G. Formation of clustered DNA damage after high-LET irradiation: a review. *Journal of Radiation Research*. 2008. Vol. 232, no. 3.
77. *Health risks from exposure to low levels of ionizing radiation: BEIR VII Phase 2*. National Academies Press, 2006. ISBN 030909156X.
78. O'CONNOR, Michael K. *Risk of low-dose radiation and the BEIR VII report: A critical review of what it does and doesn't say*. 1 November 2017. Associazione Italiana di Fisica Medica.
79. HAMZAH, Rowaidah, DEEVBAND, Mohammad Reza, GHORBANI, Mahdi, KHOSRAVI, Mehdi, POUR, Faranak Sadeghi and TAVAKOLI, Meysam. Incidence risk assessment of secondary cancer due to radiotherapy of women with rectal cancer using BEIR VII, EPA, and ICRP models. *Reports of Practical Oncology and Radiotherapy*. 2023. Vol. 28, no. 5, p. 571–581. DOI 10.5603/rpor.96870.
80. PARK, Jun Ook, NAM, Inn Chul, KIM, Choung Soo, PARK, Sung Joon, LEE, Dong Hyun, KIM, Hyun Bum, HAN, Kyung Do and JOO, Young Hoon. Sex Differences in the Prevalence of Head and Neck Cancers: A 10-Year Follow-Up Study of 10 Million Healthy People. *Cancers*. 1 May 2022. Vol. 14, no. 10. DOI 10.3390/cancers14102521.
81. COCA-PELAZ, Andrés, HALMOS, Gyorgy B., STROJAN, Primož, DE BREE, Remco, BOSSI, Paolo, BRADFORD, Carol R., RINALDO, Alessandra, VANDER POORTEN, Vincent, SANABRIA, Alvaro, TAKES, Robert P. and FERLITO, Alfio. *The role of age in treatment-related adverse events in patients with head and neck cancer: A systematic review*. 1 July 2019. John Wiley and Sons Inc.
82. JUAREZ, Jesus E., CHOI, Jehee, ST JOHN, Maie, ABEMAYOR, Elliot, TENNAPEL, Mindi and CHEN, Allen M. Patterns of Care for Elderly Patients With Locally Advanced Head and Neck Cancer. *International Journal of Radiation Oncology Biology Physics*. 15 July 2017. Vol. 98, no. 4, p. 767–774. DOI 10.1016/j.ijrobp.2017.01.209.

83. BENCHETRIT, Liliya, TORABI, Sina J., TATE, Janet P., MEHRA, Saral, OSBORN, Heather A., YOUNG, Melissa R., BURTNESS, Barbara and JUDSON, Benjamin L. Gender disparities in head and neck cancer chemotherapy clinical trials participation and treatment. *Oral Oncology*. 1 July 2019. Vol. 94, p. 32–40. DOI 10.1016/j.oraloncology.2019.05.009.
84. DICKSTEIN, Daniel R., EGERMAN, Marc, MONROSE, Erica, VARMA, Achintya, OZBEK, Umut, SHARMA, Sonam, LIU, Jerry T., GUPTA, Vishal, POSNER, Marshall R., MISIUKIEWICZ, Krzysztof, MILES, Brett A., GENDEN, Eric and BAKST, Richard L. Treatment tolerability and outcomes in elderly patients with head and neck cancer. *Head and Neck*. 1 March 2021. Vol. 43, no. 3, p. 858–873. DOI 10.1002/hed.26548.
85. GORDON, Konstantin, SMYK, Daniil, GULIDOV, Igor, GOLUBEV, Kirill and FATKHUDINOV, Timur. *An Overview of Head and Neck Tumor Reirradiation: What Has Been Achieved So Far?* 1 September 2023. Multidisciplinary Digital Publishing Institute (MDPI).
86. ZOHRI, Rouzbeh, HAHN, Lorenz, SEYEDI, Niloufar, PETERSEN, Cordula, ZIEMANN, Christian, ABEL, Jakob, KUTZ, Laura Magdalena, KRÜLL, Andreas, FLÜH, Charlotte, EHRESMANN, Carolin, ZEMSKOVA, Oksana, LIUBICH, Larysa, RADES, Dirk and LÖSER, Anastassia. Nutritional Gender-Specific Differences in Head and Neck Cancer Patients Treated with (Chemo)Radiotherapy: Results from a Prospective Trial. *Cancers*. 1 December 2024. Vol. 16, no. 23. DOI 10.3390/cancers16234080.
87. SCHUSTER, Barbara, HECHT, Markus, SCHMIDT, Manfred, HADERLEIN, Marlen, JOST, Tina, BÜTTNER-HEROLD, Maike, WEBER, Klaus, DENZ, Axel, GRÜTZMANN, Robert, HARTMANN, Arndt, GEINITZ, Hans, FIETKAU, Rainer and DISTEL, Luitpold V. Influence of Gender on Radiosensitivity during Radiochemotherapy of Advanced Rectal Cancer. *Cancers* [online]. 2021. Vol. 2022, p. 148. DOI 10.3390/cancers. Available from: https://doi.org/10.3390/cancers.https://doi.org/10.3390/cancers14010148https://www.mdpi.com/journal/cancers
88. YE, Xianghua, GUO, Dazhou, GE, Jia, YAN, Senxiang, XIN, Yi, SONG, Yuchen, YAN, Yongheng, HUANG, Bing shen, HUNG, Tsung Min, ZHU, Zhuotun, PENG, Ling, REN, Yanping, LIU, Rui, ZHANG, Gong, MAO, Mengyuan, CHEN, Xiaohua, LU, Zhongjie, LI, Wenxiang, CHEN, Yuzhen, HUANG, Lingyun, XIAO, Jing, HARRISON, Adam P., LU, Le, LIN, Chien Yu, JIN, Dakai and HO, Tsung Ying. Comprehensive and clinically accurate head and neck cancer organs-at-risk delineation on a multi-institutional study. *Nature Communications*. 1 December 2022. Vol. 13, no. 1. DOI 10.1038/s41467-022-33178-z.
89. PATHAK, Pushpraj K., VASHISHT, S. K., BABY, S., JITHIN, P. K., JAIN, Y., MAHAWAR, R. and SHARAN, V. G.G.K. Commissioning And Quality Assurance Of Halcyontm 2.0 Linear Accelerator. *Reports of Practical Oncology and Radiotherapy*. 2021. Vol. 26, no. 3, p. 433–444. DOI 10.5603/RPOR.a2021.0065.
90. BENTZEN, Søren M., CONSTINE, Louis S., DEASY, Joseph O., EISBRUCH, Avi, JACKSON, Andrew, MARKS, Lawrence B., TEN HAKEN, Randall K. and YORKE, Ellen D. Quantitative Analyses of Normal Tissue Effects in the Clinic (QUANTEC): An Introduction to the Scientific Issues. *International Journal of Radiation Oncology Biology Physics*. 1 March 2010. Vol. 76, no. 3 SUPPL. DOI 10.1016/j.ijrobp.2009.09.040.
91. WESOLOWSKA, Paulina, SLUSARCZYK-KACPRZYK, Wioletta, FILLMANN, Marta, KAZANTSEV, Pavel and BULSKI, Wojciech. Results of the IAEA supported national end-to-end audit of the IMRT technique in Poland. *Physica Medica*. 1 December 2023. Vol. 116. DOI 10.1016/j.ejmp.2023.103168.
92. SHANE. *Phantom Patient for VMAT-IMRT Verification*. [no date].

93. SHANE. *Phantom Patient for VMAT-IMRT Verification*. [no date].
94. *Absorbed Dose Determination in External Beam Radiotherapy An International Code of Practice for Dosimetry Based on Standards of Absorbed Dose to Water*. [no date].
95. *Health risks from exposure to low levels of ionizing radiation: BEIR VII Phase 2*. National Academies Press, 2006. ISBN 030909156X.
96. ARGIRIS, Athanassios, KARAMOUZIS, Michalis V., RABEN, David and FERRIS, Robert L. *Head and neck cancer*. 2008. Elsevier B.V.
97. LLEWELLYN, C D, JOHNSON, N W and WARNAKULASURIYA, K A A S. *Risk factors for squamous cell carcinoma of the oral cavity in young people Ð a comprehensive literature review* [online]. [no date]. Available from: www.elsevier.com/locate/oraloncology
98. TIPNIS, Sameer V., SPAMPINATO, Maria V., HUNGERFORD, John and HUDA, Walter. Thyroid doses and risks to adult patients undergoing neck CT examinations. *American Journal of Roentgenology*. 1 May 2015. Vol. 204, no. 5, p. 1064–1068. DOI 10.2214/AJR.14.13102.
99. BERRINGTON DE GONZALEZ, A., Gilbert, E., Curtis, R., Inskip, P., Kleinerman, R., Morton, L., ... & Rajaraman, P. Second solid cancers after radiation therapy: a systematic review of the epidemiologic studies of the radiation dose-response relationship. *International Journal of Radiation Oncology* Biology* Physics*. 2013. Vol. 86, no. 2, p. 224–233.
100. ZAREPISHEH, Masoud, URIBE-SANCHEZ, Andres F., LI, Nan, JIA, Xun and JIANG, Steve B. A multicriteria framework with voxel-dependent parameters for radiotherapy treatment plan optimization. *Medical Physics*. 2014. Vol. 41, no. 4. DOI 10.1118/1.4866886.

Appendices

Appendix 1

Summary of Head and Neck Patient

Table 11. Patient Demographics, Organ Radiation Doses (Gy), and Clinical Tumor Classification (TNM and Stage)

Patient number	Age	Gender	Esophagus	Submandibular gland (left)	Submandibular gland (right)	Larynx	Parotid_L	Parotid_R	Parotid	Spinal cord	TNM	Stage	Location
1	60	F	16.75	60.52	58.73	39.87	19.19	19.32	19.26	38.28	T4N2M0	X	Oral cavity
2	46	F	24.26	32.14	33.51	39.44	22.46	18.04	20.33	40.58	T3N2M0	IV	Oral cavity
3	72	M	15.96	1.55	1.41	37.64	0.49	0.54	0.51	40.22	T4NcM0	IV	Larynx
4	64	F	18.49	24.08	32.74	38.71	2.39	18.69	18.35	41.94	T2NbM0	X	Oral cavity
5	54	M	8.29	38.21	33.12	31.96	18.93	16.08	16.81	35.75	T4N3M0	IV	Oral cavity
6	68	M	29.15	65.93	34.53	32.64	14.8	17.03	15.95	39.08	T4aNbM0	IV	Other
7	48	M	14.84	36.81	14.6	35.35	14.54	8.22	11.07	39.46	T4NbM0	IV	Oral cavity
8	65	M	6.24	31.9	63.02	31.51	5.59	16.72	10.9	40.31	T4aNcM0	IV	Oropharanx
9	71	M	10.03	38.15	53.11	31.05	2.65	2.7	2.68	40.24	T1N0M0	IV	Oropharanx
10	78	F	1.18	58.87	50.37	43.94	14.68	18.32	16.81	43.34	T2N2M0	IV	Oropharanx
11	47	M	12.37	65.99	38.73	32.73	52.78	18.89	38.89	44.03	T2N2M0	IV	Oropharanx
12	60	F	15.96	38.62	32.17	38.53	10.55	23.39	16.06	41.54	T3N2M0	IV	Oral cavity
13	70	M	13.88	34.43	31.21	34.94	18.56	15.16	16.14	43.01	T4T2M0	X	Other
14	70	M	35.95	39.73	52.15	65.32	16.44	19.77	18.48	44.4	T4aN2M0	IV	Hypopharanx
15	60	F	7.62	6.95	27.01	12.32	5.25	18.65	19.21	19.93	T4N0M0	IV	Other
16	61	M	10.19	1.48	1.63	70.42	1.15	1.11	1.13	44.12	T3NbM0	IV	Larynx
17	56	M	1.2	49.6	33.11	35.63	18.08	40.52	32.73	34.56	T4bN2M0	IV	Oropharanx
18	65	M	11.66	58.49	34.04	32.1	15.66	19.47	17.35	42.41	T3N2M0	IV	Larynx
19	60	M	8.4	37.47	34.88	30.01	14.14	12.06	13.22	43.07	T2N0M0	II	Larynx
20	62	M	5.98	66.15	55.6	37.61	19.8	19.79	19.29	36.86	T4aN2M0	IV	Larynx
21	68	M	6.09	64.59	56.36	58.05	24.53	11.14	17.67	43.61	T2N2M0	IV	Hypopharanx
22	69	M	16.63	39.92	54.35	65.57	11.94	14.05	13.04	40.2	T2N0M0	X	Hypopharanx

Table 12. Patient Demographics, Organ Radiation Doses (Gy), and Clinical Tumor Classification (TNM and Stage) (continued)

Patient number	Age	Gender	Esophagus	Submandibular gland (left)	Submandibular gland (right)	Larynx	Parotid_L	Parotid_R	Parotid	Spinal cord	TNM	Stage	Location
23	57	M	14.47	47.32	53.18	39.29	23.03	12.01	18.08	41.78	T2N2M0	X	Oral cavity
24	73	M	7.93	38.77	16.4	17.81	9.3	24.85	19.1	29.12	T1N0M0	I	Other
25	76	F	26.3	22.36	32.6	32.82	12.42	19.71	17.22	41.28	T4aN0M0	IV	Oral cavity
26	65	M	13.64	34.11	54.71	38.71	19.76	18.71	19.3	38.56	T4N2M0	X	Oral cavity
27	60	M	23.02	32.12	30.01	10.69	27.29	18.52	17.45	43.39	T4N3M0	IV	Oropharanx
28	74	F	15.09	2.33	1.96	20.8	4.25	3.98	4.11	33.28	T4N1M0	IV	Oral cavity
29	72	F	8.47	34.75	34.38	38.93	19.15	19.59	18.1	42.26	T4aN0M0	IV	Oral cavity
30	66	M	16.64	30.11	29.7	39.59	35.96	19.1	17.74	37.86	T4aN2M0	IV	Oropharanx
31	72	M	28.64	34.64	34.91	36.99	18.83	45.84	16.3	43.39	T3N2M0	IV	Oral cavity
32	57	M	29.74	27.31	50.28	54.55	24.61	21.11	18.33	37.77	T4bN2M0	IV	Oropharanx
33	64	M	17.19	33.37	27.04	36.44	10.25	9.6	18.61	39.5	T4aN2M0	IV	Hypopharanx
34	65	M	21.36	39.32	61.2	38.81	18.76	7.73	16.61	42.42	T4aN2M0	IV	Oral cavity
35	62	M	9.1	34.6	35	35.16	17.1	17.31	18.02	40.91	T4aN2M0	IV	Larynx
36	67	F	27.48	34.62	51.1	37.93	18.9	44.36	16.65	41.75	T3NXM0	X	Oropharanx
37	57	M	17.45	31.22	60.2	36.9	19.45	19.18	14.2	43.29	T4N3M0	X	Hypopharanx
38	68	M	4.75	32.82	32.91	37.1	17.92	18.08	17.71	40.91	T4aN0M0	IV	Larynx
39	56	M	10.46	38.67	59.1	52.74	17.38	18.83	18.17	40.96	T2N1M0	III	Hypopharanx
40	65	M	32.22	54.58	35.1	35.11	10.86	13.92	12.55	40.4	T4N2M0	X	Hypopharanx
41	63	M	27.98	51.2	37.52	35.98	24.95	23.62	24.31	43.74	T4aN2M0	X	Oropharanx
42	51	F	25.93	69.84	64.45	39.61	18.84	14.86	16.68	37.19	T4aN2M0	IV	Oral cavity
43	78	M	4.74	49.9	49.54	25.7	19.66	16.45	19.03	32.38	T4aN3M0	X	Oral cavity
44	69	M	7.09	38.44	32.64	35.58	14.55	10.79	22.12	30.02	T4N2M0	X	Hypopharanx
45	64	M	11.85	35	30.65	38.26	16.53	24.81	20.16	44.65	T4bN2M0	IV	Oropharanx
46	68	F	11.23	56.42	59.58	38.58	18.91	24.43	21.75	39.96	T4aN1M0	IV	Oral cavity
47	52	M	11.44	34.87	34.11	68.97	18.08	18.29	18.2	37.46	T4aN2M0	IV	Hypopharanx
48	64	M	2.79	0.77	1.23	39.1	0.27	0.32	20.89	28.78	T2N0M0	II	Larynx
49	66	F	29.19	69.79	33.72	52.23	34.09	16.48	19.19	43.2	T3N3M0	IV	Hypopharanx
50	49	M	27.25	39.76	63.22	35.71	22.23	48.42	17.8	39.37	T4aN2M0	IV	Oral cavity

Table 13. Patient Demographics, Organ Radiation Doses (Gy), and Clinical Tumor Classification (TNM and Stage) (continued)

Patient number	Age	Gender	Esophagus	Submandibular gland (left)	Submandibular gland (right)	Larynx	Parotid_L	Parotid_R	Parotid	Spinal cord	TNM	Stage	Location
51	57	M	27.46	65.16	34.19	40.16	19.86	20.18	20.04	44.74	T3N2M0	IV	Oral cavity
52	60	M	22.42	39.04	53.28	31.15	17.82	18.21	18	37.18	T4aN2M0	IV	Oral cavity
53	74	M	13.38	57.83	56.43	37.98	15.92	17.65	16.33	43.09	T4aN2M0	X	Oral cavity
54	76	M	29.88	64.96	34.41	34.51	19.61	17.72	18.67	41.94	T4N2M0	X	Larynx
55	53	F	25.46	33.73	69.16	39.55	19.01	55.88	16.2	43.77	T1N2M0	X	Oropharanx
56	64	M	10.45	56.3	57.44	33.11	14.11	18.17	16.13	32.64	T3N2M0	IV	Oral cavity
57	60	F	16.76	60.52	58.73	39.87	19.19	19.32	19.26	38.28	T4N2M0	X	Oral cavity
58	76	M	20.88	53.04	53.7	38.62	18.88	18.82	18.85	38.95	T3N2M0	IV	Oropharanx
59	67	F	18.92	39.2	43.33	38.04	16.06	23.54	19.76	36.39	T4N1M0	X	Oral cavity
60	51	M	21.36	54.46	54.03	38.19	16.13	29.6	23.91	41.67	T4N2M0	X	Oral cavity
61	63	M	11.54	51.66	38.99	36.92	18.23	16.84	17.46	39.93	T2N3M0	IV	Larynx
62	64	M	6.69	54.45	57.12	35.12	15.5	17.59	16.54	40.48	T3N2M0	IV	Hypopharanx
63	64	M	14.4	58.07	58.55	41.31	16.18	18.62	17.01	36.37	T4aN2M0	IV	Larynx
64	64	M	32.3	37.25	33.04	34.05	17.5	13.88	15.6	34.05	T4N0M0	X	Larynx
65	67	M	7.07	53.1	55.45	34.24	17.43	18.38	17.93	38.3	T2N0M0	II	Oropharanx
66	67	F	13.38	58.56	27.18	39.35	19.28	19.92	19.63	43.33	T4bN2M0	X	Oropharanx
67	61	M	18.4	33.19	59.71	37.77	12.42	18.26	14.7	28.77	T4N2M0	X	Oropharanx
68	67	F	16.54	37.7	34.22	32.28	11.82	30.76	18.32	44.22	T3N2M0	IV	Oropharanx
69	55	M	28.07	54.07	53.46	37.11	15.77	16.35	16.06	32.37	T4bN3M0	IV	Hypopharanx
70	69	M	11.55	39.99	55.59	37.91	17.18	18.09	17.63	37.98	T4N0M0	X	Oropharanx
71	62	M	10.55	38.8	61.83	35.49	20.92	23.89	22.21	35.98	T4N2M0	X	Oral cavity
72	51	M	15.19	55.1	54.55	39.25	18.36	16.65	17.55	40.98	T1NXM0	X	Oral cavity
73	62	M	32.57	32.56	32.76	41.11	11.64	12.14	11.9	21.77	T4aN1M0	IV	Larynx
74	49	M	29.9	60.92	67.41	33.86	23.15	24.15	23.68	38.96	T4aN2M0	IV	Oral cavity
75	67	M	12.81	57.06	60.31	32.22	16.07	18.33	17.09	35.1	T3N1M0	III	Larynx
76	65	M	4.78	34.15	32.12	36.3	13.47	16.83	14.96	38.04	T4aN3M0	IV	Hypopharanx
77	60	M	28.55	30.11	34.22	40.82	19.05	19.06	17.44	42.76	T4N2M0	X	Oropharanx
78	57	M	9.74	60.91	68.7	38.74	15.7	13.91	14.81	37.96	T4N2M0	X	Hypopharanx

Table 14. Patient Demographics, Organ Radiation Doses (Gy), and Clinical Tumor Classification (TNM and Stage) (continued)

Patient number	Age	Gender	Esophagus	Submandibular gland (left)	Submandibular gland (right)	Larynx	Parotid_L	Parotid_R	Parotid	Spinal cord	TNM	Stage	Location
79	66	M	9.88	38.54	65.9	31.57	16.71	23.15	19.98	40.47	T4aN1M0	X	Oropharanx
80	60	M	18.84	33.57	32.38	37.28	18.01	17.21	17.6	41.52	T2N0M0	II	Oropharanx
81	57	F	0.57	28.2	24.67	36.21	0.63	0.64	18.54	38.57	T2N0M0	II	Larynx
82	47	M	15.74	49.18	38.63	30.39	20.97	19.64	20.33	41.28	T3N0M0	III	Oropharanx
83	65	M	9.24	60.21	2.69	28.24	19.05	15.94	19.16	43.29	T3N3M0	IV	Oral cavity
84	71	M	11.11	29.64	28.8	30.76	25.48	12.83	19.97	41.39	T2N0M0	II	Oropharanx
85	64	M	24.12	38.3	38.02	35.22	18.91	19.83	18.87	36.72	T3N0M0	III	Larynx
86	61	M	12.03	55.85	48.15	27.76	22.65	20.91	20.09	41.52	T4aN2M0	IV	Oral cavity
87	74	M	13.16	51.22	38.86	35.22	23.86	19.94	22.18	44.81	T4aN2M0	IV	Oral cavity
88	50	M	29.7	33.2	29.61	38.62	19.61	12.39	16.36	44.03	T2N2M0	IV	Hypopharanx
89	64	M	11.58	47.31	38.5	41.61	25.89	17.53	21.82	41.57	T4N3M0	IV	Oral cavity
90	56	M	31.74	34.43	60.9	34.27	18.11	22.1	20.22	41.81	T4aN2M0	IV	Oral cavity
91	66	M	9.77	50.65	50.64	32.74	23.72	30.66	23.86	43.01	T4bN0M0	IV	Oral cavity
92	67	F	16.47	36.51	32.1	36.74	21.81	24.16	22.89	39.59	T2N2M0	IV	Oropharanx
93	45	M	15.36	37.01	54.11	65.48	18.36	18.62	18.52	44.62	T4aN2M0	X	Oropharanx
94	64	M	11.24	42.1	44.33	42.99	23.92	20.57	22.16	43.24	T4bN2M0	X	Oropharanx
95	44	M	11.64	36.22	39.1	32.1	24.83	16.09	20.48	42.19	T3N2M0	IV	Oral cavity
96	79	F	5.18	33.11	61.1	37.03	22.74	22.63	11.32	44.85	T3N1M0	X	Oropharanx
97	70	M	2.31	48.59	27.82	35.44	10.31	16.46	17.99	31.78	T4bN1M0	IV	Hypopharanx
98	71	M	17.88	32.33	38.43	13.23	24	5.24	19.1	18.38	T4N2M0	X	Larynx
99	65	M	14.36	51.1	32.14	35.68	18.25	19.41	18.58	39.95	T4N2M0	X	Oropharanx
100	65	M	7.94	53.7	37.18	34.73	20.21	16.08	18.52	40.33	T4aN2M0	IV	Oral cavity
101	40	M	14.79	33.07	38.77	36.06	17.94	18.29	18.14	36.67	T2N0M0	II	Oral cavity
102	55	M	13.2	68.59	22.66	28.47	19.74	4.78	12.9	34.31	T4bN2M0	IV	Oral cavity
103	73	M	11.61	51.47	52.79	32.58	28.74	8.43	22.23	40.06	T4N3M0	IV	Oral cavity
104	53	M	28.67	38.85	37.44	33.08	16.81	19.39	18.14	43.92	T1N3M0	IV	Oral cavity
105	50	M	29.92	31.11	34.75	39.62	19.87	19.79	19.83	43.23	T3N2M0	X	Oral cavity

Table 15. Patient Demographics, Organ Radiation Doses (Gy), and Clinical Tumor Classification (TNM and Stage) (continued)

Patient number	Age	Gender	Esophagus	Submandibular gland (left)	Submandibular gland (right)	Larynx	Parotid_L	Parotid_R	Parotid	Spinal cord	TNM	Stage	Location
106	67	M	0.28	54.09	51.01	2.22	17.44	14.59	12.21	16.05	T4bN2M0	IV	Oral cavity
107	64	M	23.41	64.35	63.34	30.48	20.64	19.77	20.21	35.04	T2N0M0	II	Oral cavity
108	53	M	10.4	33.09	38.17	28.76	14.98	17.3	15.97	43.37	T4bN3M0	IV	Hypopharanx
109	53	M	11.79	33.12	37.76	27.47	22.01	12.72	18.71	31.89	T4N2M0	X	Oral cavity
110	61	M	33.16	59.83	60.78	30.87	18.58	21.06	19.86	42.34	T4bNbM0	IV	Hypopharanx
111	56	M	9.44	34.19	61.51	23.77	19.18	22.14	20.69	42.88	T2N1M0	III	Oral cavity
112	65	M	16.28	53.17	58.13	30.73	23.36	24.14	23.78	43.84	T4aN2M0	IV	Oropharanx
113	49	M	19.82	50.53	50.1	38.91	18.37	24.07	20.92	44.33	T2N2M0	IV	Larynx
114	54	M	7.69	37.97	35.82	65.55	19.34	19.61	19.48	43.64	T4aNcM0	IV	Hypopharanx
115	64	M	10.35	36.18	43.09	37.9	19.3	22.88	21.18	38.75	T4NcM0	X	Oral cavity
116	63	M	4.74	48.63	50.59	27.47	18.04	18.29	18.15	37.67	T4aN2M0	X	Oral cavity
117	69	M	5.38	32.23	64.15	30.09	21.94	24.59	20.72	40.14	T1N3M0	X	Oropharanx
118	62	M	24.67	63.01	37.33	40.01	19.02	46	34.05	39.71	T4NbM0	X	Hypopharanx

Appendix 2

Out of field doses measurement

Table 16. Measurement dose - Channel 1 (Middle)

Distance, cm	AAA			AC		
	MD	TPS	nC	MD	TPS	nC
0	0.03	0.05	0.49	0.03	0.05	0.49
2	0.04	0.05	0.72	0.04	0.05	0.72
4	0.07	0.06	1.17	0.06	0.07	1.17
6	0.14	0.12	2.63	0.19	0.24	3.49
8	1.72	1.79	31.85	1.76	2.04	32.63
10	2.05	2.04	38.07	2.08	2.03	38.65
12	2.07	2.04	38.44	2.08	2.03	38.53
14	1.92	1.97	35.69	1.97	1.77	36.60
16	1.65	1.76	30.62	1.69	1.41	31.33
18	1.33	1.35	24.76	1.31	1.29	24.36
20	1.25	1.29	23.20	1.20	1.09	22.32
22	1.29	1.26	23.93	1.23	1.37	22.91

Table 17. Measurement dose - Channel 2 (Right)

Distance, cm	AAA			AC		
	MD	TPS	nC	MD	TPS	nC
0	0.02	0.05	0.46	0.03	0.04	0.46
2	0.04	0.05	0.73	0.04	0.05	0.71
4	0.06	0.06	1.15	0.06	0.07	1.15
6	0.14	0.12	2.57	0.14	0.19	2.60
8	1.66	1.61	30.80	1.67	1.98	31.06
10	2.04	2.01	37.84	2.06	1.99	38.31
12	1.85	1.81	34.25	1.85	1.66	34.40

Table 18. Measurement dose - Channel 2 (Right) (Continued)

Distance (cm)	AAA			AC		
	MD	TPS	nC	MD	TPS	nC
14	1.79	1.73	33.31	1.84	1.69	34.07
16	1.69	1.70	31.29	1.74	1.75	32.31
18	1.66	1.69	30.74	1.68	1.56	31.12
20	1.51	1.43	28.11	1.48	1.40	27.39
22	1.71	1.73	31.87	1.72	1.72	31.92
24	1.52	1.64	28.17	1.49	1.55	27.57

Table 19. Measurements dose – Channel 3 (Left)

Distance (cm)	AAA			AC		
	MD	TPS	nC	MD	TPS	nC
0	0.02	0.05	0.46	0.02	0.04	0.46
2	0.04	0.05	0.66	0.04	0.05	0.66
4	0.06	0.05	1.03	0.06	0.06	1.03
6	0.13	0.09	2.32	0.18	0.20	3.31
8	1.54	1.63	28.63	1.56	1.87	28.9
10	1.77	1.77	32.84	1.76	1.74	32.68
12	1.73	1.63	32.04	1.73	1.69	32.13
14	1.69	1.70	31.40	1.72	1.56	31.90
16	1.54	1.49	28.55	1.59	1.53	29.43
18	1.54	1.53	28.50	1.58	1.55	29.25
20	1.51	1.52	27.99	1.55	1.56	28.79
22	1.56	1.55	28.86	1.57	1.56	29.28

Table 20. Measurement dose -Channel 4 (Spinal Cord)

Distance (cm)	AAA			AC		
	MD	TPS	nC	MD	TPS	nC
0	0.02	0.05	0.44	0.01	0.04	0.34
2	0.03	0.05	0.63	0.03	0.05	0.63
4	0.05	0.06	0.85	0.05	0.06	0.92
6	0.08	0.09	1.57	0.08	0.09	1.42
8	0.24	0.16	4.41	0.18	0.19	3.39
10	0.68	0.66	12.55	0.53	0.53	9.90
12	0.58	0.41	10.74	0.52	0.48	9.64
14	0.55	0.66	10.23	0.31	0.26	5.76
16	0.27	0.25	5.05	0.24	0.20	4.53
18	0.21	0.22	3.96	0.20	0.18	3.79
20	0.22	0.20	4.11	0.19	0.18	3.67
22	0.29	0.25	5.34	0.22	0.18	4.12